MDPI

Article

Aircraft Emissions, their Plume-Scale Effects, and the Spatio-Temporal Variability of the Atmospheric Response: a Review

Kieran Tait [1,†,‡], Firstname Lastname [1,‡] and Firstname Lastname [2,*]

[1] University of Bristol; kt16229@bristol.ac.uk
[2] Affiliation 2; e-mail@e-mail.com
* Correspondence: e-mail@e-mail.com; Tel.: (optional; include country code; if there are multiple corresponding authors, add author initials) +xx-xxxx-xxx-xxxx (F.L.)
† Current address: Affiliation 3
‡ These authors contributed equally to this work.

Keywords: keyword 1; keyword 2; keyword 3 (List three to ten pertinent keywords specific to the article; yet reasonably common within the subject discipline.)

Citation: Tait, K.; Lastname, F.; Lastname, F. Aircraft Emissions, their Plume-Scale Effects, and the Spatio-Temporal Variability of the Atmospheric Response: a Review. *Aerospace* **2021**, *1*, 0. https://doi.org/

Received:
Accepted:
Published:

1. Introduction

Aircraft act as high-altitude emissions vectors, transporting a number of radiatively and chemically active substances across vast regions of the globe. These substances induce a net global warming effect that constitutes 3.5% of global climate change due to anthropogenic emissions [1]. Two thirds of this impact result from the climate forcing of non-CO_2 emissions, primarily through emission of nitrogen oxides (NO_x), water vapour (H_2O) and particulate matter (PM). These emission species interact with ambient air through chemical and microphysical processing, giving rise to the production and depletion of radiatively active substances that perturb the net energy balance of the atmosphere (e.g. NO_x-induced ozone production, condensation trail (contrail) generation through H_2O and PM emissions etc.). The degree to which aircraft emissions induce a climatic response varies depending on the state of the background atmosphere (i.e. its chemical composition and meteorology) and the time of day and year on which emissions are released. This means that aviation climate impact is spatio-temporally sensitive, i.e. the same emissions released at different times and/or locations can lead to very different climate effects.

The dispersion of aircraft emissions occurs over great length and time scales, with emissions entrained in the aircraft exhaust plume which spreads hundreds of kilometres [2] over its lifetime of up to 12 hours [3]. The elevated concentrations of emitted chemical species present within the plume result in additional nonlinear chemical (gas-phase and heterogeneous) and microphysical processes which are not accounted for in global chemistry models, due to the inherent assumption of instantaneous dispersion (ID) of emissions. The ID assumption models emissions as homogeneously mixed into the volume of the computational grid cell to which they are released, thus neglecting any subgrid-scale nonlinear processing that may occur throughout the plume lifetime [4]. Plume-scale nonlinear effects are also further augmented in high-density airspace regions, where plumes intersect and the emissions contained within them accumulate, leading to chemical saturation. Two key saturation effects have been noted to be of particular significance with respect to aviation climate impact: (1) the saturation of NO_x emissions, which leads to decreasing ozone production with increasing NO_x concentrations [5], and (2) the dehydration of water vapour leading to diminished contrail climate impact [6]. Therefore, the atmospheric response to non-CO_2 aircraft emissions is not only sensitive to natural variations in the atmospheric state, but it is also affected

by heightened emissions concentrations due to the presence of lingering plumes from previous aircraft.

Optimising flight routes with respect to minimum climate impact (instead of minimum fuel burn) is a concept that has become prevalent in the literature in recent years. This involves re-routing aircraft to avoid particularly climate-sensitive regions of the atmosphere, based on provision of en-route chemical and meteorological information. Niklaß et al. (2019) [7] has shown through simulation efforts that it is possible to achieve a 12% reduction in climate impact at virtually no additional cost to fuel burn, evidencing the practicability of climate-optimised routing. Other studies approach this issue purely from the perspective of superimposing aircraft plumes through formation flight. The aerodynamic benefits of formation flight due to wake energy retrieval are already well established [8,9], however it has become increasingly evident that formation flight can also be used to exploit climate-beneficial saturation effects due to the superposition of plumes from aircraft involved. In Dahlmann et al. (2020) [10] a preliminary study exploring the potential for climate impact reduction due to saturation effects in formation flight and found that NO_x saturation led to a reduction in ozone production efficiency of ~5% and a mutual inhibition of contrail growth, quelling their radiative properties by 20 to 60%.

This review article documents the current state of literature on aviation's atmospheric effects and the influence of nonlinear plume-scale processing on the global net climate impact, to bring to light the notion that aviation-induced perturbations to atmospheric chemistry can simply be viewed as another constraint in the climate-optimised routing problem. Section 2 covers the emissions generation process and the methods used to model aircraft performance and emissions. Section 3 explores the dispersion characteristics of aircraft emissions on the subgrid scale, alluding to the various modelling methods developed to investigate the dynamical characteristics of aircraft plumes. In section 4, air traffic management principles and their effect on aviation emissions distribution is considered, on both the local and global scale, followed by section 5 which explores aircraft climate impact, based on the emissions released and the chemical and physical processes that occur on the grid and subgrid-scale of global models. Section 6 looks into the effect of subgrid-scale processes that occur due to emissions accumulation in high-density airspace, and finally section 7 explores potential mitigation efforts to reduce aviation-induced climate change by modifying aircraft operations, such as climate-optimal routing and formation flight.

2. Aircraft emissions

Aircraft propulsion systems provide the essential driving force component to enable powerful and efficient flight. In modern commercial aviation, responsible for ~88% of global aviation fuel usage [11], it is commonplace to use a gas turbine propulsion system operating on kerosene-based jet fuel. Aviation's environmental impact stems from the emission and dispersion of chemically and radiatively active substances that are generated during jet fuel combustion. This section details the emissions generation process and the modelling methods implemented to estimate emissions based on aircraft performance calculations and the determination of fuel consumption.

2.1. The generation of aircraft emissions

The widespread usage of kerosene-based jet fuels stems from the need to satisfy strict power-to-weight and safety requirements demanded by commercial aircraft; this is because kerosene has an exceptionally high energy density and wide operating temperature range at a low financial cost, compared with alternative fuel types [12,13]. The stoichiometric combustion of kerosene with air required to generate thrust, does however generate a number of chemically and radiatively active emission species which are emitted from the aircraft into its wake. These aircraft emissions interact with the surrounding atmosphere, perturbing the natural balance of chemistry and contributing

to air quality issues and anthropogenic climate change. The mass of emission produced per unit mass of fuel burnt is often referred to as the emission index (EI), measured in grams of emission per kilogram of fuel [g/kg].

2.1.1. Primary jet fuel combustion products

The products of jet fuel combustion are often divided into two categories: primary and secondary, alluding to the way in which they are formed inside the aircraft engine. The primary products jet fuel combustion are carbon dioxide (CO_2), water vapour (H_2O) and, due to fuel impurities, a relatively small amount of sulphur oxides (SO_x). These products are generated as a direct result of the combustion reaction that takes place, and hence depends on the carbon-hydrogen-sulphur composition of the fuel. The direct coupling of the production of these species to fuel consumption means that they have a constant EI throughout all phases of flight. Example values based on the typical chemical composition of jet fuel are given in table 1 [14].

Table 1: Emission indices estimates for CO_2, H_2O and SO_2, averaged from a range of existing studies testing various aviation fuel types [15].

CO_2	H_2O	SO_2
3.149 g/kg fuel	1.230 g/kg fuel	0.84 g/kg fuel

2.1.2. Secondary jet fuel combustion products

Further to this, a number of secondary combustion products are generated in the aircraft exhaust, namely oxides of nitrogen (NO_x = NO + NO_2), carbon monoxide (CO), unburnt hydrocarbons (HC), particulate matter (PM) and trace levels of volatile organic compounds (VOCs) [16]. These products are termed secondary, as their production levels differ depending on the nature of the combustion process and the engine load condition [17]. This means that their EIs are variable throughout flight, depending on aircraft engine type, engine operating conditions, and the atmospheric conditions of the surrounding environment [18]. NO_x emissions originate from the entry of atmospheric nitrogen (N_2) into the high temperature combustion chamber. The level of NO_x increases with increasing temperature and pressure, as it is coupled to the thermal reaction processes that occur in the primary combustion zone. Therefore, with the assumption of constant polytropic and combustion efficiencies, the emission index of NO_x ($EINO_x$) can be correlated with aircraft fuel flow [17,19]. As a result of inefficiencies in the combustion process, products such as CO and HC are formed. Contrarily to NO_x, these emissions are direct products of incomplete combustion, meaning their concentrations are inversely proportional to combustion efficiency. Since combustion efficiency correlates with thrust for sea level static (SLS) conditions, and thrust correlates with fuel flow, this means that EICO and EIHC decrease with increasing fuel flow.

PM emissions from aircraft can be categorised by their volatility: non-volatile PM (nvPM) and volatile PM (vPM). The primary source of nvPM present in aircraft exhaust is soot, which constitutes the greatest warming effect of all particles released from aircraft [20]. Soot is generated in the fuel rich regions of the combustor, where the condensation of unburnt aromatic hydrocarbons takes place, converting low carbon content HC fuel molecules into carbonaceous agglomerates containing millions of carbon atoms [21,22]. The extent of soot formation therefore depends on the fuel-air-ratio and the mixing processes that take place in the combustor, which vary with combustor design and are influenced by the non-homogeneous flow and temperature fields. Accurate measurements of these parameters are rare, making it very difficult to directly acquire quantitative data on soot emissions. Instead, soot EI can be estimated based on correlation with the so-called smoke number measured in engine certification procedures [19].

The formation of vPM from aircraft largely derives from the emission of sulphur derivatives, lubrication oil and VOCs [23]. During combustion, the sulphur content

in the fuel is mostly oxidised to sulphur dioxide (SO_2), some of which is then further oxidised to sulphuric acid (H_2SO_4) when emitted into the atmosphere. In the presence of sufficient water vapour, sulphate aerosols (SO_4) can be generated, which exhibit the largest cooling effect from aircraft PM emissions [14]. The sulphate EI is a factor of fuel sulphur content, which varies depending on fuel composition and the specific emissions characteristics of the engine [24]. Due to the low volatility of lubricant oil, the emitted oil vapour from aircraft will add to the condensed mass of VOCs and contribute to vPM concentrations. The VOCs produced either from the oxidized fuel fragments or due to the pyrolysis in the combustion chamber can also act as vPM, which may have sufficiently low vapour pressure to allow condensation in the atmosphere forming a coating on the surface of the nvPM, impacting cloud formation, precipitation and climate [14]. The particulate matter emitted near the exit nozzle plane of the combustor consists only of nvPM. However vPM are produced through nucleation and condensation downstream. Thus it is difficult to estimate the total amount of vPM produced within the exhaust plume, as the formation of vPM is dependent on the concentration of sulphates and VOCs present in the exhaust, and the distance from the combustor [25].

2.2. Aircraft emissions modelling

Accurate quantification of aircraft emissions for any given flight requires the calculation of aircraft performance to estimate the total energy consumed, and hence, the total fuel burnt throughout the flight duration. With knowledge of fuel flow rates experienced throughout flight, flow rates of aircraft emission species can be deduced based on empirical engine performance datasets and emissions models.

2.2.1. Fuel burn estimation

Computational modelling of aircraft performance allows the simulation of aircraft trajectories and the quantification of forces experienced throughout flight, enabling the approximation of thrust and fuel flow across all phases of flight. Aircraft performance models that are prevalent in academia and industry, such as the BADA (Base of Aircraft DAta) method [26] and Piano-X [27], emulate aircraft behaviour by coupling a database of aircraft-specific performance datasets to mathematical models to calculate useful flight characteristics, such as fuel flow and fuel burn, at discrete time steps during flight. This iterative approach accounts for the time-varying nature of aircraft properties like mass, speed and heading, thus leading to a more accurate estimate of performance and fuel burn estimation. Further to this, models such as the Aviation Environment Design Tool (AEDT) [28] exist, which carry out four-dimensional (4-D) physics-based simulations of aircraft trajectories at an exceptionally high spatial and temporal resolution, providing highly accurate predictions of fuel consumption and localised emissions impacts. Such tools do however come at the expense of high computational and financial cost, and often require proprietary data that is unavailable to the public domain. An alternative state-of-the-art open-source performance model that has been made available in recent years is the OpenAP model [29]. This model consists of four main components; the aircraft and engine property model, the kinematic and dynamic aircraft performance models, and utility libraries; and can describe the characteristics of 27 common aircraft and 400 turbofan engines, deeming it a feasible alternative for researchers who do not have access to proprietary data and licensing for the other more established models.

2.2.2. Calculating aircraft emissions at reference conditions

Aircraft performance models provide estimates of aviation fuel burn, but to estimate the particular chemical speciation of emissions released due to fuel combustion, aircraft emissions models must be implemented. As mentioned previously, the primary combustion products, CO_2, H_2O and SO_2, have a direct relation to the amount of fuel burnt and hence a constant EI for a given fuel composition, with standard estimates provided in table 1. Secondary combustion products such as NO_x, CO and HC however,

largely depend on operational and atmospheric conditions. Empirical relationships between EI and fuel flow for secondary combustion products have been determined at reference operating conditions using engine performance datasets, such as the International Civil Aviation Organisation (ICAO) engine emissions databank [30]. This databank was developed for the purpose of engine certification and compliance with landing and take-off (LTO) cycle emissions standards, outlined in ICAO Annex 16 Vol. II [31]. Engine test data have been collected at sea-level static (SLS), International Standard Atmosphere (ISA) conditions, for four reference operating conditions (thrust settings) relevant to the LTO cycle: take-off (100% thrust), climb out (85%), approach (30%) and taxi in/out (7%). For every engine at each of the four LTO modes, a reference fuel flow and corresponding emission index has been derived, allowing emissions to be estimated for aircraft operating under any of the four modes, to a reasonable degree of accuracy. An exemplary ICAO EI dataset is provided in table 2.

Table 2: Example ICAO engine emissions data for Rolls Royce Trent 970-84 engine [30].

	Take-off	**Climb out**	**Approach**	**Idle**
Fuel flow [kg/s]	2.605	2.157	0.720	0.255
EI NO_x [g/kg]	38.29	29.42	12.09	5.44
EI CO [g/kg]	0.32	0.31	1.16	13.38
EI HC [g/kg]	0.02	0.12	0.08	0.04

2.2.3. Calculating aircraft emissions at non-reference conditions

In reality, aircraft spend the majority of flight outside of the LTO vicinity (above 3,000 ft), and the operating conditions and atmospheric conditions vary considerably. To enable the accurate analysis of aircraft emissions outside of reference conditions, a number of emissions modelling methods have been developed. Such methods apply the necessary adjustments and interpolations to the LTO-limited engine performance datasets, to generate more realistic estimates of aircraft emissions across the whole flight profile. SAE International Aerospace Information Report 5715 (AIR5715) [32] describes a number of methods for calculating aircraft emissions throughout all modes of operation and compares their relative merits. For the primary combustion species, the Fuel Composition method is presented, which determines $EICO_2$, EIH_2O and $EISO_x$ from the proportions of carbon, hydrogen and sulphur in the fuel. The set of methods concerning the estimation of $EINO_x$, EICO and EIHC include the ICAO reference method, the Boeing fuel flow method 2 (BFFM2), the DLR fuel flow method and the P3T3 method, in order of increasing fidelity. The ICAO reference method serves as the simplest and least accurate approach, computing emissions purely based on the ICAO reference conditions, without applying corrections to account for atmospheric effects at altitude. Therefore, it is only applicable for emissions analysis of aircraft flying in the LTO region. The remaining methods, BFFM2, DLR and P3T3 can be applied at all aircraft operating conditions, including at cruise, as they apply interpolations to engine performance datasets to determine emissions indices throughout the whole duration of a flight. The BFFM2 method and the DLR method (NO_x only) are the mid-tier models, as they provide reasonable estimates of EIs purely from interpolating the EI reference data and applying corrections for atmospheric effects based on ambient meteorological data, aircraft fuel flow and Mach number. The gold standard for modelling of NO_x, CO and HC emissions is however, the P3T3 method, as it utilises detailed thermodynamic modelling data to determine the precise emission indices at any given point throughout flight. Required data includes the combustor inlet temperature (T3), pressure (P3) and the fuel-air ratio (FAR) at both reference and operational conditions. All of which are difficult to obtain without access to proprietary engine-specific performance data, which limits the accessibility of this model to open-access researchers [33,34].

See figure 1 for an example of how EIs are interpolated based on the logarithmic relationship between EI and fuel flow, using the BFFM2 method [35]. Furthermore, methods are also presented to account for the remaining key emission species, such as the Derivative Factor method [28] used to approximate the EI values for VOCs such as non-methane HC (NMHC) throughout flight and the First Order Approximation method [23] used to estimate PM emission indices. The choice of method generally depends on the emission species to be observed, the compromise between modelling resources and data availability, and the level of accuracy required.

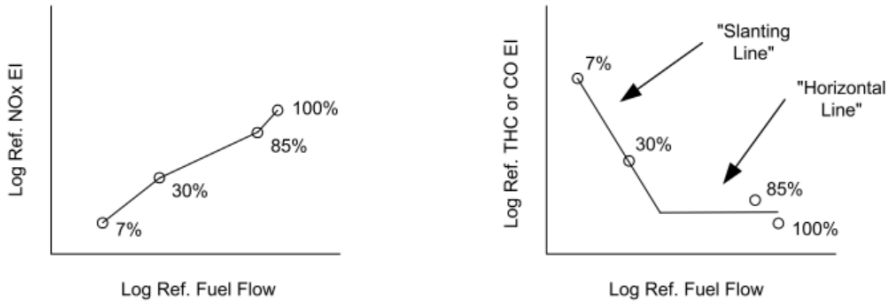

Figure 1. Example log-log plots of EI against fuel flow at reference conditions, as prescribed by the BFFM2. The percentage values refer to the thrust as a percentage of maximum thrust at SLS conditions [32].

2.2.4. Emissions inventories and integration into large-scale climate models

The estimation of aircraft emissions for a specific flight involves the simulation of aircraft performance across the entire flight profile so as to estimate fuel flow and engine operating conditions throughout flight. Knowledge of fuel flows and engine performance characteristics permits the estimation of aircraft emissions, based on the coupling of empirical engine certification data and emissions modelling methods, which interpolate the data to determine the emissions at non-reference conditions. This emissions estimation procedure is commonly carried out on a regional and global scale to determine emissions from a whole range of flights, which are then stored in so-called emissions inventories [36]. Aircraft emissions inventories collate data from all flights in the desired range and populate three-dimensional (3-D) latitude-longitude-altitude grid cells (e.g. $1° \times 1° \times 1000$ ft) with total emissions quantities [4].

Aircraft emissions inventories are utilised to model the atmospheric effects of aviation, using large-scale atmospheric models that captures the chemistry, physics and dynamics of the Earth-atmosphere system (see section 5.3 for further detail on climate modelling approaches). Such models allow one to simulate the perturbation to the state of the atmosphere due to an input of emissions and, in turn, provide quantitative indicators that enable modellers to determine the resultant climate impact (e.g. concentrations of key greenhouse gases, aerosol formation and distribution, cloud processes etc.) [37]. However, one underlying issue with this conventional approach to aviation climate modelling, is that the use of gridded emissions data inherently assumes the instantaneous dispersion (ID) of emissions into the atmosphere [38]. The ID approach assumes that aircraft emissions are instantaneously dispersed into the latitude-longitude-altitude computational grid cell in which they were released. The dimensions of this grid cell are solely determined by the spatial resolution of the global model, and hence do not serve as an accurate physical representation of emissions dispersion.

In reality, emissions released from aircraft are confined to the aircraft exhaust plume, which inhibits mixing with the surrounding atmosphere for up to a day after emission. Throughout this time, a number of nonlinear chemical and microphysical processes occur, due to the elevated concentrations of emissions species in the plume. These nonlinear plume-scale processes affect the eventual climate response to these emissions, yet most regional and global aviation climate impact studies [39] often neglect the presence of

the aircraft exhaust plume and opt for the simplified ID method. The following section explores the dynamical evolution of emissions following their release into ambient air, and discusses modelling approaches present in the literature which can be implemented to represent plume-scale effects in large-scale models. Such modelling is, however, often set aside due to computational issues associated with resolving consistency between the two model resolutions.

3. The dispersion of aircraft emissions and the aircraft exhaust plume

Following their expulsion into the free atmosphere throughout flight, aircraft exhaust gases are confined to a plume that undergoes a series of dynamical regimes (**jet**, **vortex**, **dispersion** and **diffusion** regimes), before becoming fully diluted in the surrounding air. The entrainment of emissions within the plume throughout these dynamical regimes leads to initial species concentrations that are several orders of magnitude higher than background levels [40], giving rise to a number of nonlinear chemical and microphysical effects. These plume-scale effects have considerable implications on the eventual chemical composition of the surrounding atmosphere and lead to the formation of aerosols and ice crystals in the aircraft wake. Therefore, inclusion of plume-scale effects is vital for high fidelity modelling of aviation's impact on the climate.

3.1. Plume-scale dynamical regimes

In order to accurately account for nonlinear effects experienced in the aircraft exhaust plume, one must first understand the dynamical response of the plume after combustion, to gauge the length and time scales over which aircraft emissions are entrained within it.

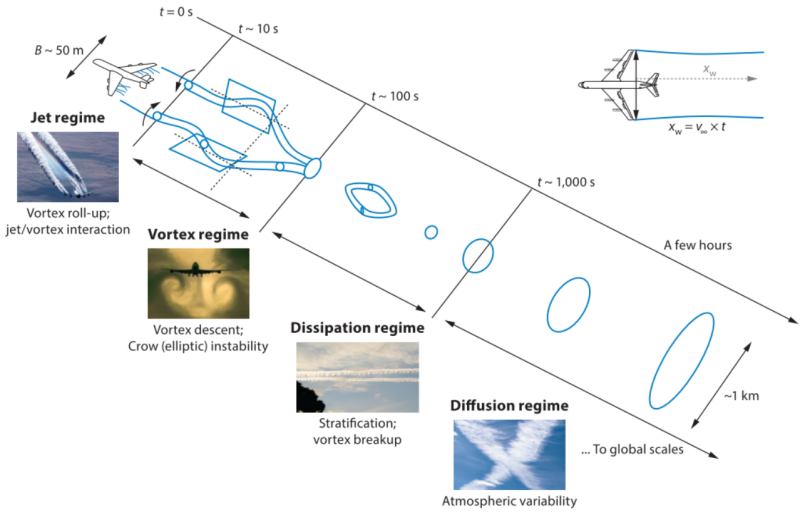

Figure 2. Aircraft exhaust plume dynamical regimes. Wake distance behind aircraft $x_w = v_\infty \times t$ where v_∞ is aircraft speed and t is the post emission time [41,42].

Exhaust gas temperatures range from around 1500 K post combustion, 600 K at engine tailpipe, followed by mixing with bypass air cooling the flow to around 300 K [16] as the dispersion process begins. During the first 1–20 s post emission, an axisymmetric jet is formed, which rapidly diffuses into ambient air and cools to ambient temperatures. Over this period, known as the **jet** regime, the airflow passing over the wings is diverted downwards to generate lift, thus creating a vortex sheet at the trailing edge of the aircraft. This vortex sheet rolls up into a pair of counter-rotating vortices which are shed at the wing tips. The evolving vortex pair then merge together and propagate downwards, due to their mutually induced downwash velocity, trapping the exhaust plume within their cores and signalling the beginning of the vortex regime.

Throughout the **vortex** regime, which occurs between 20 s and 2 minutes after combustion, the primary wake containing the vortices and trapped exhaust plume sinks by around 150–200 m, resulting in a slight temperature increase of 1–3 K, due to the adiabatic heating of exhaust constituents in the sinking vortices. Further to this, the organised vortical structure means the wake does not grow significantly during this time, and hence the concentrations of entrained chemical species remain relatively constant. The adiabatic heating of the exhaust does however lead to baroclinicity at the border between each vortex and the ambient air, which detrains some momentum, heat and exhaust constituents from the primary wake, to form a secondary wake. This secondary wake trails upwards as it is warmer than the surrounding ambient air, and it escapes the influence of the vortex structure, resulting in enhanced mixing with ambient air and thus experiences different chemical and microphysical processes compared with the primary wake [42].

Following this is the **dispersion** regime, in which the aircraft-induced dynamics subside due to the growth of Crow instability [43], which dissipates and disintegrates the primary and secondary wake vortices [41]. The breakdown of the organised vorticial structure and the production of turbulent motion leads to a sudden increase in the rate of entrainment between the exhaust plume and the ambient air by a factor of 10, therefore giving rise to a continuous decay of concentration and temperature within the plume. This regime lasts for 2–5 minutes after combustion, however this varies as the strength of aircraft induced vortices is proportional to the weight and span, and inversely proportional to the speed of the aircraft [42]

Lastly, the plume undergoes its final dynamical event, known as the **diffusion** regime. This regime is characterised by the aircraft-induced dynamics becoming negligible (after about 6 minutes [44]), followed by the subsequent dominance of atmospheric processes in the spreading of the aircraft exhaust plume and its constituents. Atmospheric turbulence, radiation transport and stratification are examples of natural phenomena that contribute to the diffusion of the plume, with total dilution to ambient concentrations often occurring over timescales of 2–12 h post emission [3]. During this time, the plume may spread up to a few kilometres through atmospheric turbulence and shear in the ambient air, diluting the exhaust species over vast volumes of airspace [45].

Plume-scale climate effects that result from the confinement of emissions to the aircraft exhaust plume during the four dynamical regimes considerably alter the eventual global warming effect of a particular flight, and therefore should be appropriately accounted for in modelling efforts to estimate aviation's climate impact.

3.2. Plume-scale modelling

To tackle the issue of neglected plume-scale effects in the computational analysis of aviation-induced climate change, a number of plume modelling methods of varying fidelity have been theorised in the literature. Sub-grid resolution plume models simulate the dynamical response of the aircraft plume, so as to capture the nonlinear chemistry and microphysical effects that occur within it. The outputs of plume models can then be parametrised into low-resolution global models, to increase the accuracy of climate impact calculations through better accounting of the emissions dispersion process.

3.2.1. Empirical dilution model

Plume dynamics control the rate at which aircraft emissions mix and dilute into the surrounding atmosphere, directly affecting the resulting climate impact of aircraft emissions due to the nonlinear effects experienced in the plume, before it becomes homogeneously mixed into the ambient air. Quantifying the rate of dilution and modelling the climate effects that occur within aircraft plumes is therefore an essential process in the accurate analysis of aviation's climate impact [45]. In Schumann et al. (1998) [46], an empirical dilution model was developed to investigate the mixing rate of plumes throughout their typical lifetimes, based on data collated from over 70 aircraft exhaust

353 plume encounters with research aircraft. The characteristic property observed in this
354 study is the plume dilution ratio, N, which is defined as the amount of air mass that
355 the exhaust plume generated from a unit mass of fuel burn, mixes with, per unit flight
356 distance within the bulk of the plume.

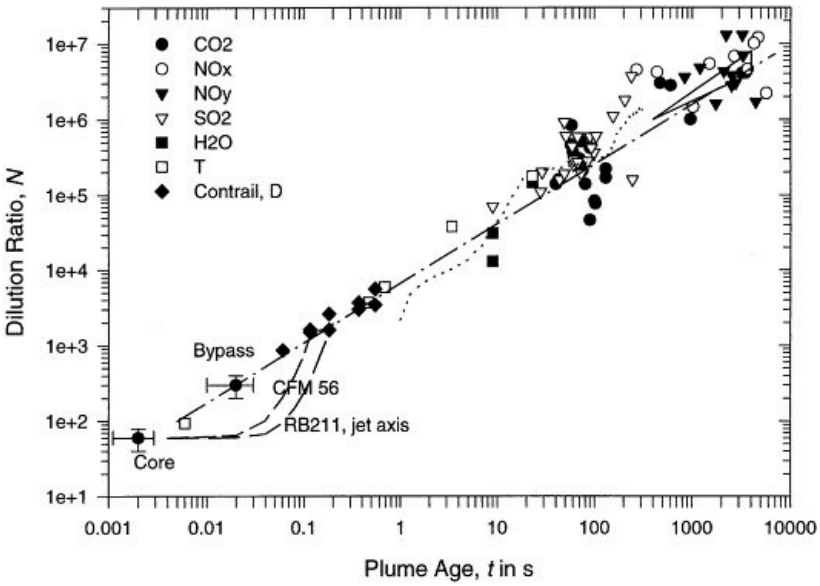

Figure 3. Dilution ratio against plume age derived from empirical data. Marker shapes correspond to tracer species as displayed in legend. Markers with error bars correspond to characteristic values for the engine core (leftmost and lower) and bypass exits (rightmost and upper). The dashed curves near the core represent dilution on the jet axis, calculated for two engine types: CFM56 and RB211. The dotted curve represents large eddy simulation results from Gerz and Ehret (1997) [47]. The range of dilution values computed for large plumes ages by Dürbeck and Gerz (1996) [48] are bounded by the triangle, top right of the figure. The dash-dotted line shows the interpolation that is represented by equation (1) [46].

357 In figure 3, measured dilution ratios from the plume encounters are plotted against
358 plume age. The data was generated by measuring the concentrations of a range of
359 chemical sources across a variety of aircraft types, within the time interval of 0.001–
360 10,000 s. The significance of these findings is that, in spite of the diverse range of
361 chemical species and aircraft types observed, throughout all four dynamical regimes,
362 a relatively consistent logarithmic relationship emerges between dilution ratio and
363 increasing plume age. When interpolating the regression line fitted to the data in figure
364 3, the following equation can be obtained where N represents dilution ratio, t is plume
365 age in seconds, and t_0 serves as an arbitrary reference scale.

$$N = 7000(t/t_0)^{0.8},\ t_0 = 1s \tag{1}$$

366 It is evident from the figure however, that encounters with plumes older than
367 50–100 s tend to diverge from the line fit, indicating a reduction in accuracy of the loga-
368 rithmic approximation over time. This is likely due to the transition from the organised
369 vortex structure present in the vortex regime, to the turbulent dispersion regime, where
370 more unpredictable atmospheric processes begin to take place and become the primary
371 influence on the evolution of the plume. Therefore, this empirical model can only be
372 used reliably up to the vortex regime. Beyond this, a Gaussian approximation to the
373 distribution of species concentrations is typically employed, accounting for dispersion
374 effects experienced at cruising altitudes, such as advection, gravitational sedimentation,
375 anisotropic diffusion, wind shear and stable stratification [49]. Two popular modelling
376 methods which implement Gaussian approximation and the two-dimensional diffusion

equation to model aircraft plumes over their whole lifetime are the Single Plume model and its discretised counterpart, the Multi-layered Plume model.

3.2.2. Single and Multi-layered Plume models

The Single Plume (SP) model, first presented in Petry et al. (1998) [38], approximates the time-evolving concentration field of an aircraft exhaust plume using a Gaussian distribution [50]. Petry represents diffusion through eq. (2), a differential equation that describes the temporal variation of exhaust concentration C of species i in the plume

$$\frac{\partial C_i}{\partial t} = -sz\frac{\partial}{\partial y}C_i + D_v\frac{\partial^2}{\partial^2 z}C_i + D_h\frac{\partial^2}{\partial^2 y}C_i + 2D_s\frac{\partial^2}{\partial y \partial z}C_i \tag{2}$$

This two-dimensional diffusion equation is a function of wind shear (s), horizontal (y) and vertical distance from plume centre (z), and the horizontal (D_h), vertical (D_v) and shear (D_s) diffusion coefficients, as calculated based on empirical data recorded under typical atmospheric conditions at aircraft cruising altitudes and assuming a horizontal flight path [51]. The solution to the diffusion equation is a time-varying Gaussian function, with standard deviations σ_h, σ_v and σ_s that depend on s, D_h, D_v, D_s, time t and the respective initial values ${\sigma_{0h,v}}^2$

$${\sigma_h}^2(t) = \frac{2}{3}s^2 D_v t^3 + (2D_s + s{\sigma_{0v}}^2)st^2 + 2D_h t + {\sigma_{0h}}^2, \tag{3}$$

$${\sigma_v}^2(t) = 2D_v t + {\sigma_{0v}}^2, \tag{4}$$

$${\sigma_s}^2(t) = sD_v t^2 + (2D_s + s{\sigma_{0v}}^2)t. \tag{5}$$

The standard deviations of the Gaussian function can then be used to deduce useful parameters such as plume cross-sectional areas and concentrations. Outputs such as these can serve as input to atmospheric models, enabling the simulation of the dynamical evolution of the plume, and its entrained emissions throughout its lifetime.

The main drawback of the SP model however, is the assumption of homogeneous concentration distribution throughout the plume at any given time. This homogeneity assumption is sufficiently accurate up to the vortex regime, where plume cross-sectional areas are relatively small, entrainment rates are low, and the mixing ratio is relatively consistent across the plume diameter [52]. However, beyond this, the spike in entrainment rates following the breakdown of vortices causes rapid plume expansion, and the drop in concentration from plume core to outer edges becomes increasingly significant [53,54]. This spatial concentration gradient along the plume cross-section cannot be captured using the SP approach, so an alternative model is proposed, known as the Multi-layered Plume (MP) model, as seen in figure 4. The MP model builds upon the SP model by discretising the plume cross-section into a number of concentric rings, enabling the inhomogeneous concentration profile to be represented by varying the mean concentration in each ring.

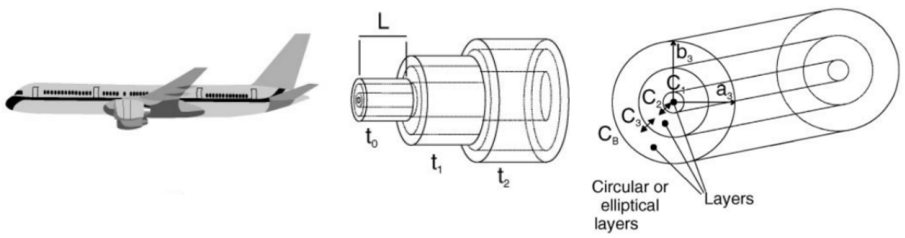

Figure 4. MP model visual representation [2]. Plume length L was set to the distance travelled over 1 s (247 m in this scenario) with three out of eight concentric rings shown for each timestep. $C_1 - C_3$ indicate the concentrations in each ring and the arrows represent mixing between the layers.

As Kraabol et al. (2000a) [2] states, the Gaussian approximation to emissions dispersion only applies to the dynamical evolution of passive species, and is not suitable for modelling the evolution of chemically active species, due to the nonlinear chemical response in the plume. To counteract this issue, this paper implements an adapted version of the MP model, in which the plume is divided into 8 concentric rings, each with a chemistry module incorporated to estimate the chemical production and loss mechanisms of all species present. Applying this model under assumed turbulent conditions derived from Dürbeck and Gerz (1996) [48], graphs of horizontal and vertical plume radius are plotted against plume age, as shown in figures 5. After just 1 hour, it is predicted that plumes can spread between 1 and 10 km horizontally, whilst only reaching around 50–100 m vertically due to atmospheric stratification [51]. As the plume approaches the end of its typical lifetime, between 10 and 15 h, plume cross-sections can reach 100–200 km horizontally and 200–400 m vertically. The vast length scales over which plumes span throughout their lifetime provides ample evidence to suggest that, in high-density airspace, plumes can overlap. The overlapping of plumes can thus lead to spikes in emissions concentrations that exceed that of single aircraft plumes, thus augmenting nonlinearities in the climate response and further propagating discrepancies between plume and global model outputs [55].

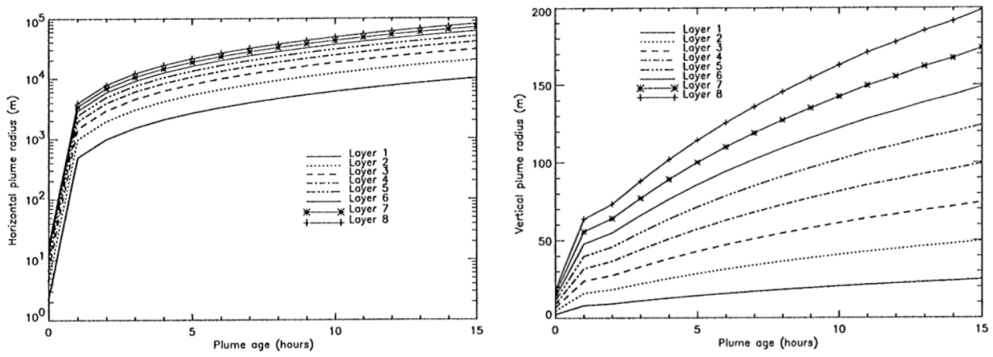

Figure 5. Evolution of **(a)** horizontal and **(b)** vertical plume radius over time, for MP model under assumed turbulent conditions [**?**].

3.2.3. Aircraft Plume Chemistry, Emissions, and Microphysics Model (APCEMM)

Models such as APCEMM from Fritz (2018) [56] further increase the accuracy of the SP and MP models by capturing additional effects that affect plume evolution and hence the resultant climate response once the plume is fully diluted. This includes effects such as plume anisotropy and asymmetry which impact the eventual spatial distribution of the plume, and modelling of the microphysical processes that strongly influence contrail formation and persistence. The model is similar to the MP model in that a chemistry module is simulated in a number of concentric rings which have differing concentration fields, that decrease with increasing radial distance from the plume core. The rest of the computation (i.e. mixing and microphysics) is peformed on a high-resolution Cartesian grid [57]. The primary aim of this model development was to bridge the gap between the simplified Gaussian approximation and more comprehensive large eddy simulations, as elaborated on in the following subsection.

3.2.4. Large eddy simulations (LESs)

Finally, the plume dynamical evolution can be most accurately captured using high-resolution LESs over the entire lifetime of the plume. LESs can model dynamics on a scale of several millions of grid points for a few seconds to a few minutes of plume age, providing unmatched levels of accuracy at the cost of extremely high computational demand. For this reason, LESs are usually limited to case studies from which the data

obtained can be used to derive and calibrate plume parametrisations for use in the lower fidelity methods [58].

In Dürbeck and Gerz (1995) [51], LES data are used to calculate effective diffusion coefficients and plume cross-sectional properties for plume modelling purposes. The data obtained from the simulations is said to have agreed with Schumann et al. (1995) [45], where the horizontal and vertical plume scales and respective diffusivities are estimated from experimental data captured by a research aircraft measuring NO concentrations. Moreover, LESs have been used to determine plume properties on much shorter timescales in Unterstrasser et al. (2014) [44]. In this paper, plume evolution is analysed for the jet and vortex period up to 6 minutes, whilst aircraft-induced dynamics dominate; concentration profiles and plume cross-sectional areas are determined for a range of atmospheric conditions, varying stratification, turbulence, wind shear and aircraft properties. Similarly in Paoli (2008) [59], detailed LES numerical simulations are carried out for the jet and vortex phase, confirming hypotheses surrounding aerosol and microphysics modelling. These studies exemplify the use of LES methods to validate experimental findings, and serve as a means of calibration for plume model parameters that represent real-life plume dilution characteristics.

4. Air traffic and emissions distribution

The previous section discussed the forces of flight and the generation and dispersion of aircraft emissions, from the perspective of a single aircraft. However, the state of the atmosphere is inhomogeneous with respect to space and time, meaning that the climate sensitivity to aircraft emissions differs considerably, depending on the time and location of their release. Furthermore, in airspace regions where traffic density is high, aircraft fly in close proximity and their exhaust plumes may intersect, giving rise to nonlinear local climate effects that must also be considered in aviation climate analysis. Therefore it is useful to explore the influence of air traffic management and spatial and temporal demand on the distribution of air traffic, and hence its associated emissions.

4.1. Air traffic management

Air traffic management (ATM) is the system of services responsible for overseeing the network-wide implementation of safe, orderly and efficient air traffic flows, providing assistance to aircraft in transit from departure to destination aerodrome. It is the role of the air traffic control (ATC) team to manage and monitor air traffic in their respective airspace in real time, ensuring that optimum safety, order and efficiency of aircraft operations are maintained at all times [60].

4.1.1. Air traffic safety

The inherent risk involved in the transportation of vast numbers of passengers at near transonic speeds through the upper atmosphere means that aviation safety is of paramount importance. A safe aircraft operation takes the path of least danger, primarily influenced by the need to avoid unfavourable atmospheric conditions and to prevent conflicts with other aircraft [61,62]. In-flight atmospheric conditions susceptible to icing, turbulence or the presence of hazardous convective weather can all be classified as unfavourable for aircraft, with the latter presenting the greatest constraint on aircraft routing [63,64]. The increased risk resulting from flight through weather-affected regions means that aircraft must re-route, leading to restrictions on available airspace and deviations from the optimal flight profile, thus increasing flight-times, fuel burn and delays [65].

The safety risks associated with aircraft-to-aircraft collisions necessitate air traffic controllers to impose safe separation standards between aircraft in the lateral, longitudinal and vertical direction, as specified in [66]. The stated minimum separation distances between aircraft are 5 nautical miles (NM) laterally, 20 NM longitudinally and 1,000 ft in the vertical direction under the most lenient scenarios. A breach of separation

laws in more than one direction is known as a conflict and must be resolved as quickly as possible. The enforcement of separation minima therefore introduces a theoretical upper limit on airspace density, i.e. the number of aircraft that occupy a fixed volume of airspace at any one time.

4.1.2. Air traffic order

To keep air traffic flows organised within controlled airspace, aircraft are ordered to follow the traditional fixed-route air traffic network, constructed from four key airspace elements that facilitate the air traffic management process [60]:

- **airports/aerodromes** - an area of land or water intended to be used for the arrival, departure and surface movement of aircraft;
- **waypoints** - a specified geographical location used to define the flight path of an aircraft, representing either a navigational aid (navaid) or a reference coordinate that the aircraft must fly by or fly over;
- **airways** - a controlled portion of airspace established in the form of a corridor (usually 8-10NM wide) between two waypoints;
- **sectors** - a region of airspace managed by a single ATC team, stratified into various levels to accommodate a wide variety of traffic.

In [67], the notion of optimising air traffic flows for a given demand and capacity is explored, in which air traffic flows are represented using these four key elements. **Airports** represent the sources and sinks of the flow, **airways** are the arcs along which the flow travels, **waypoints** are the network nodes at which airways intersect, merge or diverge, and **sectors** are a collection of waypoints and contiguous segments of airways. The fixed-route network restricts airspace availability even further, due to the discretisation of flight levels and the requirement to pass specified waypoints [68,69]. This can lead to particularly high frequencies of aircraft passing through high-density airspace, potentially leading to congestion along busy airways and waypoints where airways intersect resulting in inhomogeneities in the distribution of air traffic and potential congestion along high-density airways.

4.1.3. Air traffic efficiency

The third and final component of effective air traffic management is the optimisation of flight trajectories, subject to the prioritisation of safety and the compliance with the fixed-route airspace structure. Flight trajectory optimisation is an essential step in ensuring maximum airspace utilisation and efficiency, so that revenue is maximised and demand levels are sufficiently met. Trajectory optimisation is a multi-faceted problem, requiring consideration of nonlinear aircraft performance, wind and weather forecasts, payload, departure fuel load, reserve fuel load and ATM constraints that restrict aircraft operations and routing [70]. This requires an exhaustive assessment to be carried out at the flight planning stage, to test all possible combinations of route, payload, fuel load and operating approach, involving tens to hundreds of thousands of calculations per flight. The most optimal scenarios are then ranked in order of optimality, with the final route selected based on operator preference and/or the occurrence of unexpected circumstances, such as sudden adverse weather conditions or aircraft conflicts [71].

In an ideal airspace situation where the atmosphere is calm and constant; aircraft are not constrained to a fixed route; and there is no risk of conflict with other aircraft, the least-time and least-energy aircraft operation would be to fly the great-circle arc between departure and destination. The vertical profile of the aircraft would consist of a continuous climb out to the most efficient cruise altitude, then to cruise at constant speed, with the ability to cruise-climb continuously as the aircraft burns fuel and loses mass. In reality, the true optimal route can deviate considerably from the great-circle arc, instead taking the path which minimises the risk of bad weather encounters and collisions, abides by the fixed-route airspace structure, whilst also flying a route which is optimised with respect to wind and temperature. The magnitude and direction of wind and the

548 localised variation in temperature experienced by the aircraft throughout flight, can
549 have a drastic impact on route optimality, with tailwinds and colder temperature regions
550 being favourable [72]. Ng et al. (2012) [73] found for a wide range of wind-optimal flight
551 scenarios that domestic flights saved up to 3%, and international flights saving up to
552 10% on both fuel burn and travel time, despite flying longer routes. Furthermore, the
553 vertical flight profile of the aircraft must adhere to flight level allocations, meaning that
554 step climbs must be performed as fuel is burnt, further condensing air traffic and its
555 corresponding emissions into narrow bands of altitude.

556 #### 4.1.4. Airspace capacity

557 The effective management of air traffic relies on the human cognition of air traffic
558 controllers to make difficult decisions and carry out complex tasks in a time-critical
559 dynamic environment. This includes ensuring safety through avoidance of poor atmo-
560 spheric conditions and conflicts with other aircraft, maintaining order by flying along
561 the fixed-route airspace network, and optimising air traffic flows with respect to wind
562 and weather. As density and complexity levels of air traffic increase, so does the mental
563 workload of the air traffic controller, up until a threshold level is reached where the
564 controller can no longer safely handle the situation. The maximum number of aircraft
565 permitted by the ATC team in charge of a particular airspace volume is known as the
566 airspace capacity, and is driven by the airspace situation, state of equipment being
567 used, and the controller's own mental state [74]. Airspace capacity is limited more by
568 controller workload than is it separation laws, meaning human cognition is the true
569 limiting factor on the number of aircraft that can occupy a particular airspace volume
570 at a particular time [68,75]. Therefore, models of controller workload are often used to
571 estimate airspace capacity, in which ATC tasks are modelled to determine a safe upper
572 limit on workload. In Welch et al. (2007) [75], a macroscopic workload model is pro-
573 posed which generalises ATC tasks into four distinct categories: background, transition,
574 recurring and conflict tasks. This provides an objective basis for estimating capacity
575 and enables the formulation of an analytical relationship between airspace capacity and
576 sector volume, as seen in figure 6.

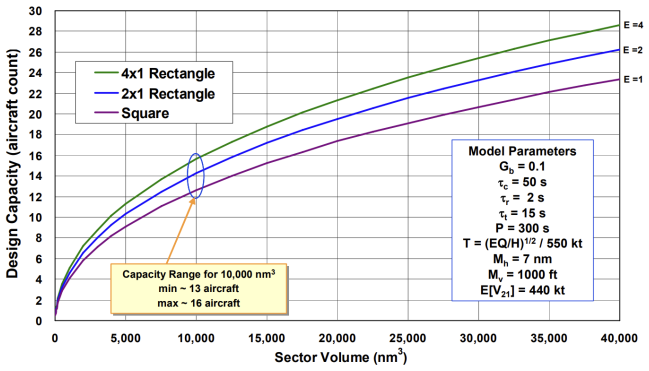

Figure 6. Aircraft capacity estimation against sector volume for a range of airspace scenarios [75]. E refers to the length to width ratio of the sector, G_b, τ_C, τ_r and τ_r are all empirical parameters related to controller workload, P is the mean task recurrence period per aircraft, T is the sector transit time, M_h and M_v are the designated horizontal and vertical separation minima between aircraft within the sector and $E[V_{21}]$ is the typical aircraft closing speed [76].

577 The capacity estimation model from figure 6 predicts that, for a 10,000 NM^3 rect-
578 angular sector of dimensions 156 NM (length, ratio 4:1) $\times$ 39 NM (width) $\times$ 10,000 ft
579 (height), a maximum of 16 aircraft may be present at any one time. In a purely hypo-
580 thetical situation where separation laws dictate capacity and all aircraft are travelling in
581 one direction lengthways, the sector could support a maximum of 490 aircraft, assuming
582 a separation of 5 NM laterally, 20 NM longitudinally and 1,000 ft vertically. This em-

phasizes the sheer extent to which human factors limit the ability to maximise capacity, and highlights the need for airspace modernisation to increase automation, integration and collaboration in the ATM system, enabling the further increase in capacity levels towards minimum separation capacity [77].

4.2. Global air traffic and emissions distribution

The nature of air traffic and emissions distribution was investigated in Olsen et al. (2013) [78] where a range of global aircraft emissions datasets are compared (NASA-Boeing 1992, NASA-Boeing 1999, QUANTIFY 2000, Aero2k 2002, AEDT 2006 and aviation fuel usage estimates from the International Energy Agency) to show distribution patterns in the latitudinal, longitudinal and vertical sense. Further to this, temporal variations with respect to both the diurnal (time of day) and seasonal (time of year) cycles are explored.

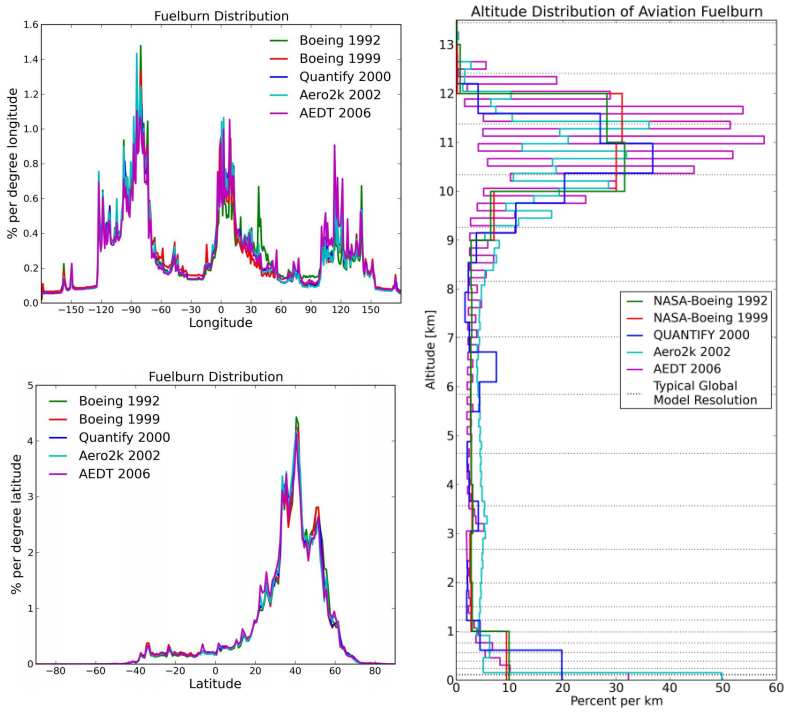

Figure 7. Spatial (latitude, longitude and altitude) distribution of global aviation fuel burn from a range of aircraft emissions datasets [78].

The climate sensitivity of the atmosphere is highly variable depending on the exact latitude, longitude and altitude combination, because of the spatially varying chemical and meteorological state of the atmosphere (e.g. [79–81]). Accurate accounting of spatial distribution patterns of air traffic is therefore very important in the estimation of aviation climate impact. Figure 7 shows the spatial distribution of fuel burn across the range of datasets in the longitudinal, latitudinal and vertical directions. The longitudinal distribution shows three emissions peaks around the densely-populated regions of the US, Europe and East Asia, with the largest situated above the North American land mass. It is evident in the latitudinal distribution, that the Northern Hemisphere dominates, with a strong peak in the northern mid-latitudes that appears due to high volumes of air traffic above the US and Europe, as well as along the connecting region of airspace, the North Atlantic flight corridor (NAFC). Contrarily, there are almost no emissions present in southern latitudes below 40°S, with the region between 40°S and the equator constituting only a small percentage. The altitudinal distribution on the other hand, experiences emissions peaks around both the low altitude LTO area and the high-altitude cruising regions between 9 to 13 km, with relatively low emission intensities at mid-

altitudes. Furthermore, the peak around cruising altitude is discretised into peaks every other flight level, due to the vertical separation constraints and the allocation of aircraft to specific flight levels, thus owing to further increases in emissions intensities at these altitudes.

The presence of diurnal and seasonal variations in key chemical and meteorogical parameters throughout the atmosphere has been widely investigated in the literature (e.g. [82]). The diurnal and seasonal variation in aviation fuel burn from Olsen et al. (2013) [78] is displayed in figure 8. The temporal fluctuations in both the state of the atmosphere and the distribution of fuel burn and emissions allude to the fact that the climate sensitivity to aircraft emissions is always changing, and therefore these parameters must be under constant observation to ensure accurate determination of global climate effects from aviation. The diurnal cycle of global aviation fuel burn, as seen on the left hand side of figure 8 displays a peak at around 15:00 UTC, which decreases through the night until around 09:00 UTC where total fuel burn begins to increase again. With regards to seasonal variation, there is significant variance between emissions datasets, however in general, all display a wintertime minimum between December and January, and a summertime maximum between June and September.

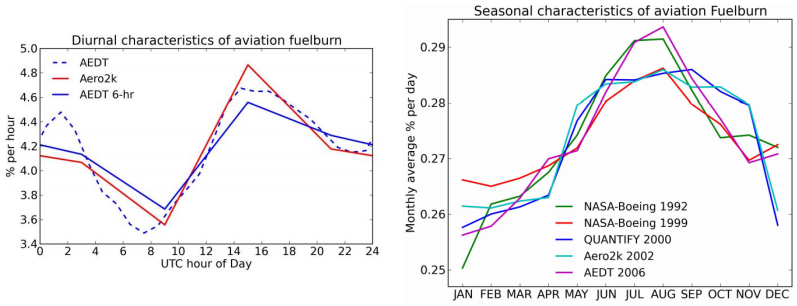

Figure 8. Temporal (diurnal and seasonal) distribution of global aviation fuel burn expressed as percentage from a range of aircraft emissions datasets [78].

4.3. Local air traffic and emissions distribution

Due to the fixed-route nature of airspace, aircraft tend to fly along common airways or flight corridors, and pass common waypoints along their journey, leading to exceptionally high flux densities of aircraft through these regions at peak times. This has implications on the nonlinear chemical and physical effects occurring at the plume scale, due to the intersection of aircraft plumes and the elevated exhaust gas concentrations entrained within them. A prime example of a high-density airspace region is the NAFC, made up of a series of tracks that aircraft traversing the North Atlantic must follow, updated daily to allow for convective weather avoidance, tracking of the North Atlantic Jet Stream and favourable tailwinds to maximise efficiency [83]. The annually-averaged number of aircraft traversing the NAFC per day has increased from 800 in 1997 [84] to around 2,500 in recent years [85], owing to the tripling of passenger demand since then [86]. With North Atlantic air traffic being confined to a limited number of tracks (usually three or four), it can be assumed that aircraft separation distances and airspace capacities are pushed to their limit on a regular basis along this and other popular flight corridors around the world.

Previous experimental work on air traffic emissions in the NAFC was carried out in the late 1990's, through campaigns such as the Pollution from Aircraft Emissions in the North Atlantic Flight Corridor (POLINAT) and Subsonic Assessment Ozone and Nitrogen Oxide Experiment (SONEX) [87]. At least 20 follow up papers were published following these campaigns, in which POLINAT/SONEX data are utilised to provide insight on a number of major scientific issues [88]. A noteworthy publication with regards to localised emissions impacts is Schlager et al. (1997) [55], which carries out an in-situ investigation of air traffic emissions signatures (nitrogen oxides (NO_x), sulphur

dioxide (SO_2) and cloud condensation nuclei (CCN)) in the NAFC using experimental data from a POLINAT research flight. The research aircraft flew perpendicular to the major eastbound corridor tracks and took measurements of various chemical concentration fields and meteorological parameters throughout. The results show that the superposition of aircraft exhaust plumes led to peak concentrations of NO_x, SO_2 and CCN above background levels by factors of 30, 5 and 3, respectively. This is because plume dispersion timescales greatly exceed the daily frequency with which aircraft emissions are input into the flight corridor, resulting in an inhomogeneous concentration field with narrow and sharp peaks over a relatively low and smooth background level [87].

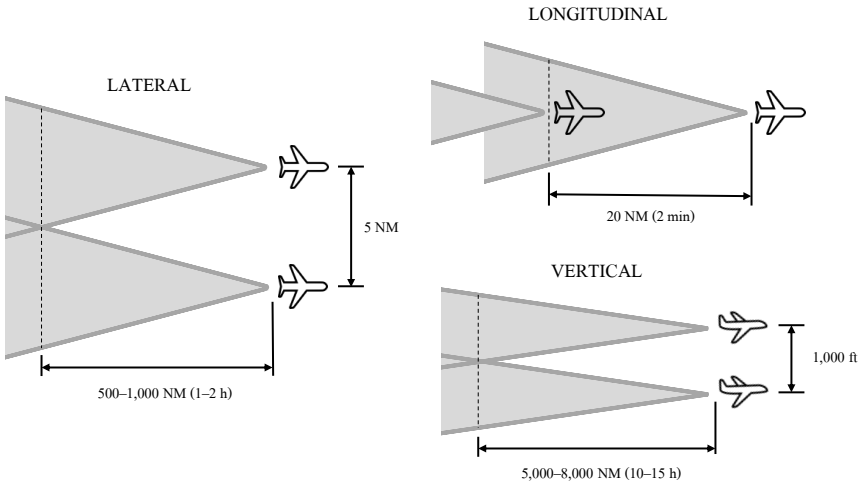

Figure 9. Lateral, longitudinal and vertical maximum plume overlap scenarios, based on nominal separation minima [66]

In the observation of plume-scale climate effects in high-density airspace regions, aircraft separation minima determine the minimum possible distance between aircraft and hence the maximum possible overlap between aircraft exhaust plumes. The degree of plume overlap influences the magnitude of emissions saturation, further accentuating nonlinear plume-scale climate processes that occur, as elaborated on in section 6.4. Using plume dimension estimates from Kraabol et al. (2000a) [2], maximum plume overlap scenarios can be inferred. Figure 9 displays the lateral, longitudinal and vertical maximum overlap scenarios for aircraft cruising at 550 kt. The longitudinal separation scenario proves to be the most effective formation for superimposing aircraft plumes, with the intersection time simply equalling the time taken to travel the separation distance between the two aircraft. For lateral and vertical superposition, the intersection time is much longer, as it is determined by the plume expansion rate in that particular direction, up until the midpoint between the two aircraft is reached. For lateral plume overlap to occur, the plumes must expand horizontally to a radius of 2.5 NM (15,190 ft), whereas for vertical, the distance is a mere 500 ft. Despite the drastic reduction in distance, the vertical plume overlap takes about an order of magnitude longer than lateral, because vertical plume expansion is substantially suppressed in comparison due to stable atmospheric stratification counteracting vertical motion [45]. In reality, air traffic flows are much more complex and the controlled and orderly formations shown in figure 9 are unlikely to occur naturally. However, the premise still holds that plume overlap occurs most frequently in congested flight corridors such as the NAFC, when aircraft travel along similar tracks and the vertical displacement between aircraft is minimal.

The importance of safety, order and efficiency in the air traffic management process and the characteristics of global and local air traffic flows have been discussed. As the

following section will explore, the atmospheric response to aviation emissions is highly sensitive to time and location, because the instantaneous state of the atmosphere (i.e. the chemical composition and meteorological situation at that particular time and position) determines the production, loss and radiative response of key chemical species that induce climatic effects [37]. With insight into how air traffic and emissions are dispersed locally and distributed globally, the contribution of aircraft emissions to climate change can be more rigorously evaluated.

5. The global climate impact of aviation

Aircraft emissions induce climate effects by perturbing the flux of inbound shortwave (SW) solar radiation and outbound longwave (LW) terrestrial radiation emitted from the Earth's surface through absorption and scattering processes that give rise to warming or cooling of the atmosphere [89]. Climate metrics such as radiative forcing can be used to measure the climate contribution of each individual emission species, enabling the determination of the net global warming effect from aviation. This section explores the potential global impact of aviation deduced from measurement and modelling of atmospheric processes.

5.1. Aircraft emissions in the Upper Troposphere and Lower Stratosphere

As figure 7 suggests, the vast majority (~60%) of aviation fuel burn and hence aviation emissions, occur at cruise altitudes, between 9 and 13km vertically. The region of the atmosphere encompassing this volume of airspace is known as the Upper Troposphere and Lower Stratosphere (UTLS), with bounds of $\pm$5 km above and below the conventional tropopause [90]. Around 20–40% of total aircraft emissions are released in the LS [14,91] and the rest are released in the troposphere, extending from the surface at take-off to the UT at aircraft cruise altitudes. The greenhouse effect due to the release of chemically-active substances in the UTLS is considerably greater than that of emissions at the surface. This is because the climate in the UTLS is more sensitive due to increased residence times of pollutants, lower background concentrations (meaning emissions have a greater influence on the atmospheric chemistry), lower temperatures, and a higher radiative efficiency [92]. Johnson et al. (1992) [93] further validates this claim, with model results concluding that NO_x emissions constitute a 30 times greater climate impact in the UT compared to equivalent surface emissions, due to the absence of direct deposition and slower conversion to stable reservoir species at aircraft cruising altitudes.

Despite such a large proportion of air traffic emissions being released into the LS region, it is thought that the perturbation to the chemical and radiative state of the stratosphere is negligible, as the vast majority of species emitted into the stratosphere are transported downwards into tropospheric regions, where they interact with the atmosphere there [94–96]. Henceforth, this review will primarily focus on the tropospheric response to aircraft emissions, except for water vapour, where the stratospheric climate response becomes particularly noteworthy.

5.2. Radiative forcing of aircraft emissions

High altitude emissions from aviation impact the climate through a variety of climate forcing pathways. Some greenhouse gases such as CO_2 and H_2O are emitted directly, others are produced indirectly through chemical processing of aircraft, such as the reaction of NO_x with atmospheric trace species to catalyse ozone production and methane destruction. Water vapour and PM emissions are responsible for the formation of high ice clouds known as condensation trails (contrails), which often trap outbound LW radiation within the atmosphere more efficiently than they reflect inbound SW radiation. PM emissions also have the potential to induce a climate perturbation through direct radiative processes due to aerosols, which may warm or cool the climate depending on the particle's optical and microphysical properties [94]. Diversity in the climate forcing pathways for each emission species means that the only reliable method

of determining the severity of each climate contribution is to model the atmospheric response and determine the resulting impact on the radiative flux of the atmosphere [16].

The most common climate metric used to compare the magnitudes of climate impact from a range of emission species is radiative forcing (RF). RF is defined as the perturbation to the net energy balance of the Earth-atmosphere system due to natural or anthropogenic factors of climate change, measured in watts per square metre [Wm^{-2}] [97]. A positive RF means that the climate forcing mechanism is inducing a warming effect and vice versa. Lee et al. (2021) [1] presents an updated analysis of the global effective radiative forcing (ERF) contributions for aviation-induced climate change. ERF is a newly proposed climate modelling framework that builds upon the RF concept by removing rapid atmospheric adjustments that bear no relation to the long-term surface temperature response that occurs over decadal timescales [89]. ERF serves as a more suitable equivalency metric to compare the global warming response of heterogeneously distributed short-lived climate forcers and uniformly distributed long-lived climate forcers. Figure 10 displays the ERF and RF contributions for each of the key aviation-induced climate forcers.

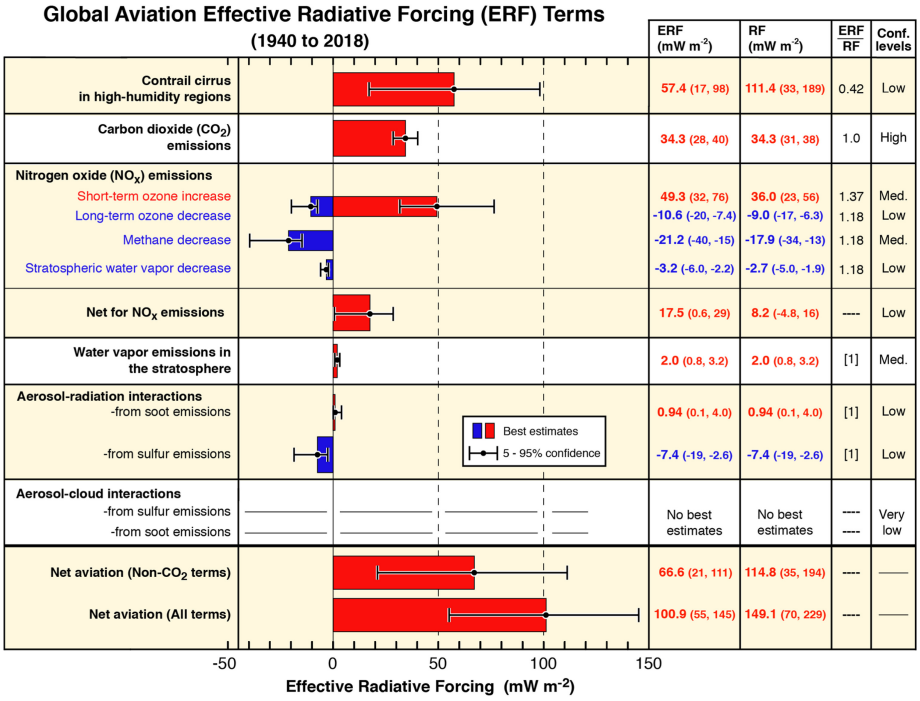

Figure 10. Radiative forcing contributions from global aviation between 2000 and 2018 [1]. Error bars represent 5–95% confidence interval, with corresponding RF and ERF values shown in parentheses.

5.2.1. CO_2

The climatic effects of aviation CO_2 emissions are direct and well understood, with the thermal absorption of outbound LW radiation leading to warming through the planetary greenhouse effect [98]. Carbon dioxide from aircraft constitutes the second largest ERF term in figure 10 at 34.3 mWm^{-2}, and the thermodynamic and photochemical stability of CO_2 means it has a relatively long atmospheric lifetime, on the order of 100 to 1,000 years [99]. This means that carbon emissions from aircraft simply serve to increase its atmospheric concentration, leading to the eventual distribution over global spatial scales. The ubiquitous and intuitive nature of CO_2-related warming deems it a suitable benchmark to compare warming from non-CO_2 climate forcers against. The assumption of instantaneous dilution in global models is sufficient for modelling the climate impact due to carbon dioxide, as it exists over vast spatial and temporal scales, meaning the

climatic effects occurring on plume time scales are negligible compared with the impact induced over its entire lifetime [4].

5.2.2. Contrail cirrus

When emissions of water vapour and PM are released into the aircraft exhaust plume in the cold and moist condition of the UTLS, the water vapour condenses around the particulates due to the high relative humidity (RH), then freezes due to the low external temperatures, permitting the formation of ice crystals. The accumulation of ice crystals in the aircraft wake gives rise to the generation of a condensation trail, also known as a contrail. Contrails have a significant level of opacity and occur at high altitudes, tending to absorb outbound terrestrial radiation more efficiently than they reflect inbound solar radiation. This induces a globally averaged ERF of 57.4 mWm^{-2}, meaning, despite their relatively short lifetime in comparison, the current contrail effect contributes more to climate change than the accumulation of aviation carbon, since the dawn of aviation [100]. Contrail evolution, i.e. how it grows, disperses and persists with time, is largely determined by the ambient conditions of the surrounding atmosphere, with lower temperatures and higher humidities generally leading to a more persistent and damaging contrail [101]. The formation and persistence of contrails can be predicted purely from the thermodynamic assumption that, as the hot and moist exhaust mixes with the colder and drier ambient air, a contrail will form if the plume exceeds water-saturation at any point and the temperature is low enough for ice nucleation to occur. A contrail will persist in the atmosphere if it mixes with air that is supersaturated with respect to ice, i.e. an ice-supersaturated region (ISSR) [102].

The thermodynamic constraints for contrail formation and persistence were first theorised by Schmidt (1941) [103] and Appleman (1953) [104], based on prior empirical observations [105], that led to the promulgation of the so-called “Schmidt-Appleman (SA) criterion". The SA criterion shows that the contrail formation threshold is purely dependent on ambient pressure, relative humidity, and the ratio of water and heat released into the exhaust plume, assuming isobaric mixing between exhaust emission and full dilution into the ambient atmosphere [106]. See Tait (2020) [107] for a detailed description of how the SA criterion can be illustrated on a plot of water vapour partial pressure against temperature. Contrails which surpass water saturation, but do not settle in ice-supersaturated air are generally assumed to be short-lived, as the ice sublimates and deposits into the surrounding atmosphere. However, contrails released into ISSRs, where the ambient humidity is higher than the saturation humidity over ice surfaces, instead grow with time because the ice particles experience deposition of surrounding water vapour molecules [101]. Persistent contrails can sometimes transition to contrail cirrus, either building onto existing cirrus clouds or forming new ones, spreading over vast swathes of the atmosphere [108] and inducing significant radiative effects. ISSRs occur frequently at aircraft cruising altitudes and often span hundreds of kilometres horizontally, however only reach depths of 100 to 1,000 m [109,110]. Their shallow nature means that aircraft can avoid them by changing flight level by $\pm$2000 ft to minimise persistent contrail generation for a minor additional fuel penalty [111].

Contrails exhibit radiative forcing through the obstruction of both SW and LW radiative fluxes, with areal coverage and optical depth (opacity) being the key drivers of contrail climate impact [112]. A contrail’s emissivity (ability to absorb and re-emit infrared LW radiation back towards Earth) and reflectance (ability to reflect inbound SW radiation back out to space due to scattering at visible wavelengths) is a function of contrail optical depth and ice particle microphysics. Contrails and other high ice clouds often warm the climate, as their thin optical depth means partial transparency to solar radiation, whilst their high ice density traps infrared radiation within the atmosphere effectively [102]. Contrail RF also displays a distinct diurnal trend; at night, contrails always induce a warming effect, as there is no SW scattering to counteract the LW absorption. During the day, contrails display a reduced net warming effect and

perhaps even a net cooling effect, depending on the amount of solar radiation that is redirected back out to space [113]. The SA criterion can be used to predict formation and persistence of contrails, however accurate quantification of contrail RF requires sufficient microphysical modelling, to deduce key information on the underlying formation mechanisms and physical and optical properties the contrail exhibits throughout its evolution [114]. See section 6.3 for elaboration on the microphysical processes that determine a contrail's radiative characteristics, and how these processes can be parametrised for modelling purposes.

5.2.3. Net-NO_x

Nitrogen oxides (NO and NO_2) released from aircraft are not radiatively active and therefore do not induce an immediate climate impact at the point of emission. Their chemical instability does however mean that they exhibit a number of indirect RF effects, due to the chemical reactions that occur following dilution into the ambient atmosphere. The chemical interactions between NO_x and trace species in the background atmosphere at aircraft cruising altitudes are highly non-linear and thus, the net-NO_x RF contribution is dependent on the instantaneous atmospheric state (time of day and year, latitude, background chemical composition, meteorological situation) [52,115].

Emissions of NO_x in the troposphere initially leads to the short term local increase in ozone production efficiency (O_3) on the time scale of weeks to months. In addition, elevated NO_x and O_3 levels lead to increased hydroxyl radical (OH) production, which in turn, leads to the long term global destruction of ambient methane (CH_4) over the time scale of decades [116–118]. The short term increase in O_3 generates a strong positive ERF of 49.3 mWm^{-2}, whereas the long term CH_4 depletion causes a lesser negative ERF of -21.2 mWm^{-2} in comparison, however there are a number of secondary negative radiative effects arising from methane depletion that must also be accounted for. This is the reduction in stratospheric water vapour (15% CH_4 RF magnitude) and a decrease in long-term background ozone in the troposphere (45% CH_4 RF magnitude), resulting from reduced background CH_4 concentrations [119,120]. Despite the long-term negative cooling effects, the short term warming from O_3 dominates, leading to a largely positive net ERF of 17.5 mWm^{-2} overall, as seen from figure 10. Section 6.1 explores the nonlinear NO_x-O_3 relationship further through explanation of the gas-phase photochemical processes that begin in the aircraft plume and are eventually distributed to regional and global scales.

5.2.4. Water vapour

The direct radiative effects induced by aviation water vapour emissions in the troposphere are insignificant, because the influence on background concentrations is negligible when compared with the natural fluxes of the Earth's hydrological cycle [14]. Any tropospheric water vapour emissions tend to get lost through deposition, due to high humidity and precipitation in this region, leading to a lifetime of around 9 days. On the contrary, water vapour that is emitted into the stratosphere (without getting transported downwards into the UT) can induce a considerable effect on the surrounding environment, due to extreme dryness at these altitudes [121]. This is because increases in stratospheric water vapour (SWV) concentrations impact the climate directly through the greenhouse effect, as well as through influences on the gas-phase and aerosol chemical composition, leading to depletion of ozone and altering the formation and growth of polar stratospheric clouds [122]. The combined impact of the direct greenhouse effect and indirect impacts on ozone and PSC due to increased SWV leads to an overall ERF of 2.0 mWm^{-2}.

As proposed in Lee et al. (2010) [94], the relatively small climate perturbation due to aviation-induced SWV has the potential to increase drastically as future flight concepts begin to take shape. This includes the environmental implications associated with the potential replacement of the current subsonic aircraft fleet with a supersonic high-speed

civil transport (HSCT) fleet, that primarily operates in the stratosphere (e.g. [40,123–125]). Furthermore, the prospect of transitioning the entire subsonic kerosene-based commercial fleet to a hypothetical fleet of cryoplanes (hydrogen-powered aircraft with zero carbon emissions) would increase aviation H_2O emissions by a factor of ~2.5 [126]. In the high-humidity conditions of the UT, this implies a considerable increase in contrail production, whereas in the LS, this would induce significant perturbations to SWV concentrations.

5.2.5. Aerosol effects

Aviation aerosol particles, either emitted directly post combustion, or formed in the wake of the aircraft, can perturb the energy balance of the atmosphere directly, as well as indirectly through the formation of contrail ice particles and heterogeneous chemical processing. The direct aerosol effect is primarily produced by the key non-volatile and volatile PM emissions; soot and sulphate aerosols.

Soot exhibits a direct radiative forcing as it has the strongest absorption of light at visible wavelengths per unit mass, more than any other abundant substance in the atmosphere, thus contributing to global heating through absorption of inbound solar radiation and light rebounded off reflective surfaces such as snow and ice [127]. The resultant heating of the atmosphere and reduction of sunlight can affect the hydrological cycle and large-scale circulation patterns, having potentially larger implications on the climate than previously thought. Despite its ability to strongly absorb sunlight, aircraft soot is responsible for only a few percent of total atmospheric black carbon, meaning the aerosol-radiation interaction brought about by aviation soot only constitutes a minor ERF of 0.94 mWm^{-2}.

Sulphur dioxide (SO_2) is formed when sulphur, which is present in hydrocarbon jet fuels, oxidizes during the combustion process [128]. SO_2 that is emitted from the aircraft exhaust can be oxidised to form gaseous sulphuric acid (H_2SO_4), which may condense on existing particles or contribute to new particle formation in low-condensation environments, resulting in sulphate aerosol formation. Sulphate aerosol is mainly composed of sulphuric acid and corresponding salts such as ammonium sulphate. The optical properties of sulphate mean that it tends to scatter inbound sunlight, thus leading to a net negative (cooling) of 7.4 mWm^{-2}, that sways the net direct climate impact of aviation aerosols towards cooling.

It is relatively well established that aviation-induced aerosols have a direct impact through radiative interactions, as discussed in this section, as well as indirectly through activation of water vapour on PM emissions through contrail formation. There are however, potentially large indirect consequences of aerosol particles interacting with cloud droplets and ambient ice particles nucleation on the aerosol surface. These effects are left without ERF estimates in figure 10, as there is great uncertainty around the accuracy of cloud process modelling and the ability to distinguish aircraft-induced clouds and natural clouds [129].

5.3. Global climate modelling

Quantifying aviation's global climate impact requires the use of computational climate models to predict the atmospheric response to the emission species released by aircraft. Climate models simulate the climate system through mathematical representation of established physical laws (e.g. conservation of mass, energy and momentum) and a plentiful supply of empirical data obtained through real world observation and measurement of physical and chemical quantities (e.g. chemical concentrations, meteorological parameters) [130]. Gridded aircraft emissions inventories are used as input to climate models [78,131], in which emissions are homogeneously distributed throughout the entire grid cell that they are released into (i.e. the ID approach). The chemistry, physics and dynamics of the atmosphere are captured in the model, along with the perturbation to the atmospheric state due to emissions, providing an output of the

spatial and temporal distributions of chemical species. Radiative transfer schemes can then be used to quantify the climate response to the perturbed chemical composition through instantaneous metrics such as RF and ERF. The variability in chemical and radiative properties of climate forcing species does however vary considerably with time. For example, CO_2 is distributed globally and affects the climate gradually over centuries, whereas contrails induce a severe yet short-lived, localised radiative impact [1]. Therefore, metrics such as Global Warming Potential (GWP, GWP*) and Global Temperature Potential (GTP) have been developed to better account for the temporal variation of certain properties, providing a more well-rounded analysis of the climate contributions of aircraft emission species [97,132,133].

There are two main climate model distinctions for use in aviation climate modelling; general circulation models (GCMs) and chemistry-transport models (CTMs). GCMs are highly sophisticated, yet very complex, as they are what are known as "online" models, calculating chemical composition, temperature and transport circulation simultaneously and in real time. This is often computationally expensive and may require very long processing times to run, depending on the simulation. CTMs on the other hand are reduced order "offline" models, calculating chemical composition based on pre-determined GCM results or empirically observed temperature and transport circulation data [14]. Example usage of GCMs in aviation climate modelling include the European Centre HAmburg Model (ECHAM) [134] for analysis of future contrail cirrus radiative forcing [135] and the Community Atmosphere Model version 5 (CAM5) [136] to comprehensively represent aviation aerosol climate impact [20]. CTMs appear much more frequently in the literature due to their versatility and computational efficiency. For example the UK Meteorological Office CTM STOCHEM [137] coupled with the Common Representative Intermediates (CRI) chemical mechanism [138] is used for modelling the global impact of aviation NO_x emissions on ozone production [35], MOZART CTM [139] for use in investigating the trade-off between CO_2 and NO_x emissions [140], and another six CTMs are presented in [14] for aviation climate impact modelling purposes. Various model intercomparison studies provide an up-to-date, elaborate review of the models available for UT and LS (and thus aviation) climate modelling [141].

6. Nonlinear plume-scale climate effects

As detailed in the previous section, the global contributions to aviation radiative forcing have been relatively well quantified. However, much of the modelling processes used to estimate these contributions are derived from global models assuming instant dispersion, thus excluding subgrid-scale chemical and physical effects that occur in the first 2–12 h upon release into the atmosphere. This section reviews current scientific understanding of these plume-scale processes, and highlights their emerging relevance in increasingly high-density airspace regions, as the accumulation of chemically active emission species further propagates the nonlinear atmospheric response.

6.1. Gas-phase photochemistry

The ultimate chemical composition of the troposphere is largely influenced by the removal of natural and anthropogenic trace species (e.g. CH_4, CO, O_3) through oxidation reactions with atmospheric free radicals, primarily the hydroxyl radical (OH), which are relatively short-lived and in low concentrations owing to their fast reactivity [142,143]. The relative abundance of OH in the troposphere controls the degree of removal of ambient trace species, otherwise known as the atmosphere's oxidative capacity. In the purely hypothetical situation where gas-phase radical chemistry was absent and hence the oxidative capacity of the atmosphere was zero, the levels of many harmful pollutants would continue to rise unabated, resulting in a drastic change in the chemical, biological and radiative state of the Earth-atmosphere system [144]. OH is produced via atmospheric photochemistry and photolysis; sunlight-initiated reaction of photolabile molecules to produce highly reactive species and/or radical species. Ozone is photolysed

by ultraviolet light ($\lambda < 320$ nm) to produce excited singlet oxygen $O(^1D)$ (R1), which then produces 2 hydroxyl radicals in the presence of sufficient levels of water vapour (R2).

$$O_3 + h\nu(\lambda < 320\,nm) \longrightarrow O(^1D) + O_2 \quad (R1)$$

$$O(^1D) + H_2O \longrightarrow OH + OH \quad (R2)$$

Understanding the influence of OH and the oxidative capacity of the upper troposphere is critical for the environmental analysis of aircraft emissions, as the closely-coupled chemical scheme involving hydroxyl and hydroperoxy radicals ($HO_x = OH + HO_2$) and nitrogen oxides ($NO_x = NO + NO_2$) determines the production and loss of key climate forcing species such as ozone and methane.

Most oxidation processes that occur in the troposphere are photochemical reaction schemes involving HO_x, and are therefore only applicable in daylight conditions due to the reliance on solar actinic flux [37]. There are however a range of chemical processes mainly involving nitrate radicals, that are potentially important for nighttime tropospheric oxidation processes involving key climate forcing species. See Jenkin et al. (2000) [145] for further elaboration on nighttime tropospheric chemistry.

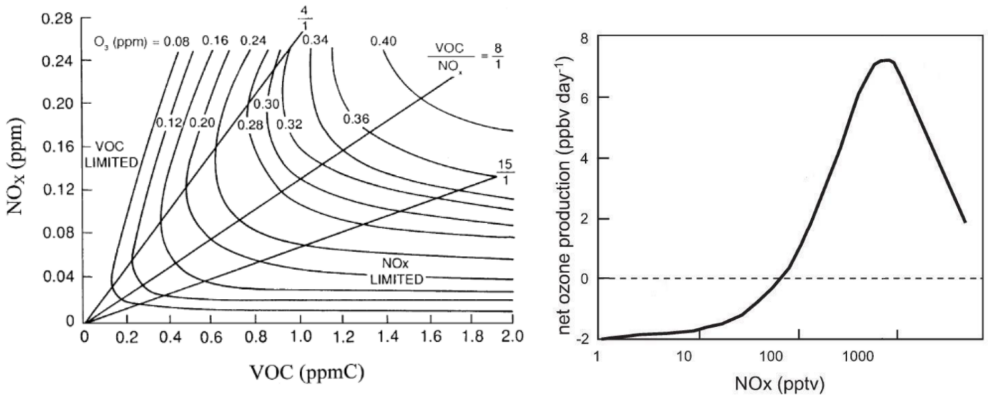

Figure 11. (a) Example isopleth diagram displaying peak ozone concentrations calculated from various initial concentrations of NO_x and a specified VOC mixture, using the US EPA empirical kinetic model [145,146]. **(b)** Schematic representation of the variation of net ozone production efficiency with NO_x concentrations, with magnitudes reflecting clean free tropospheric conditions (i.e. low VOC/NO_x ratio) [143].

Figure **??** from Jenkin et al. (2000) [145] is an exemplary ozone isopleth diagram that illustrates the O_3-NO_x-VOC relationship. At typical aircraft cruising altitudes (i.e. UTLS), where the emissions of NO_x have a significant influence on atmospheric chemistry, it is likely that VOC content is very low relative to the background NO and NO_2 concentrations. Therefore, it is likely that typical VOC/NO_x ratios are low in the UTLS, meaning that under the assumption of constant VOC concentrations, the NO_x-O_3 relationship takes a form similar to figure **??**.

6.1.1. Low-NO_x regime

In unpolluted environments characterised by low NO_x concentrations, such as in regions where the ambient air is unperturbed by aircraft emissions, the dominant reaction pathway of OH is to react with CO (~75%), with the remainder reacting with CH_4 [147]. The dominant reaction pathway therefore involves the oxidation of CO to form CO_2, as in reaction (R3) (for a detailed description of both the CO and the CH_4 oxidation cycles in low NO_x conditions, see Wasiuk (2014) [35]). In this CO oxidation cycle, produced atomic hydrogen (H) then reacts with oxygen to form HO_2 (R4), which

subsequently reacts with O_3 to form OH in the background troposphere (R5). This initiates a chain sequence in which OH and HO_2 interconvert through the termination of ozone (R6). This clean condition scheme therefore limits pollutant build up in the unpolluted upper troposphere and keeps ozone levels under control [148].

$$OH + CO \longrightarrow H + CO_2 \tag{R3}$$

$$H + O_2 + M \longrightarrow HO_2 + M \tag{R4}$$

$$HO_2 + O_3 \longrightarrow OH + 2\,O_2 \tag{R5}$$

$$OH + O_3 \longrightarrow HO_2 + O_2 \tag{R6}$$

Net reaction:

$$OH + CO + 2\,O_3 \longrightarrow CO_2 + HO_2 + 2\,O_2 \tag{R7}$$

Alternatively, HO_2 can react with itself to form hydrogen peroxide (H_2O_2) (R8), or with organic peroxy radicals such as the methyl peroxy radical (CH_3O_2) to form organic hydroperoxides (R9). These reaction pathways can become an effective sink for HO_x under most conditions, because the formation of peroxides prevents further HO_x interconversion [149].

$$HO_2 + HO_2 + M \longrightarrow M + O_2 + H_2O_2 \tag{R8}$$

$$CH_3O_2 + HO_2 \longrightarrow CH_3O_2H + O_2 \tag{R9}$$

6.1.2. NO_x-limited regime

In polluted environments, where NO_x levels are raised considerably above ambient concentrations (e.g. typical aircraft cruising altitudes), CO oxidation takes place through reactions (R3) (R4), however in the presence of nitrogen oxides, ozone is produced rather than depleted. Peroxide formation reactions (R8) and (R9) compete with the oxidation of NO to NO_2 (R10) for available HO_2 concentrations. When the latter reaction prevails, NO_2 photolysis takes place, converting back to NO with ground state oxygen $O(^3P)$ forming as a byproduct (R11). Subsequently, $O(^3P)$ reacts with atmospheric oxygen to produce O_3 (R12).

$$HO_2 + NO \longrightarrow OH + NO_2 \tag{R10}$$

$$NO_2 + h\nu(\lambda < 420\,nm) \longrightarrow NO + O(^3P) \tag{R11}$$

$$O(^3P) + O_2 + M \longrightarrow O_3 + M \tag{R12}$$

Net reaction:

$$CO + 2\,O_2 \longrightarrow CO_2 + O_3 \tag{R13}$$

Additionally, the methane oxidation cycle leads to net ozone production in the presence of NO_x. The oxidation of methane by OH produces water vapour and the methyl radical (CH_3) (R14), which further reacts with oxygen to form CH_3O_2 (R15). The produced methyl peroxy radical can then react with NO to form NO_2 through reaction (R16).

$$OH + CH_4 \longrightarrow H_2O + CH_3 \tag{R14}$$

$$CH_3 + O_2 + M \longrightarrow M + CH_3O_2 \quad \text{(R15)}$$

$$CH_3O_2 + NO \longrightarrow CH_3O + NO_2 \quad \text{(R16)}$$

$$CH_3O + O_2 \longrightarrow HO_2 + HCHO \quad \text{(R17)}$$

Net reaction:

$$CH_4 + 2\,O_2 \longrightarrow HCHO + O_3 \quad \text{(R18)}$$

The methoxy radical (CH_3O) produced can form additional HO_2 and formaldehyde (HCHO) through reaction (R17), which is then capable of reacting to form further NO_2 through reaction (R10). The resultant NO_2 produced through reactions (R16) and (R10) consequently produces ozone through the same pathway as CO oxidation (i.e. NO_2 photolysis (R11) followed by reaction of the $O(^3P)$ photoproduct (R12)). The net reaction of methane oxidation in polluted environments therefore results in positive ozone production. Figure 12 is a visual representation of the NO_x-O_3-CO-CH_4 oxidation reaction scheme described thus far.

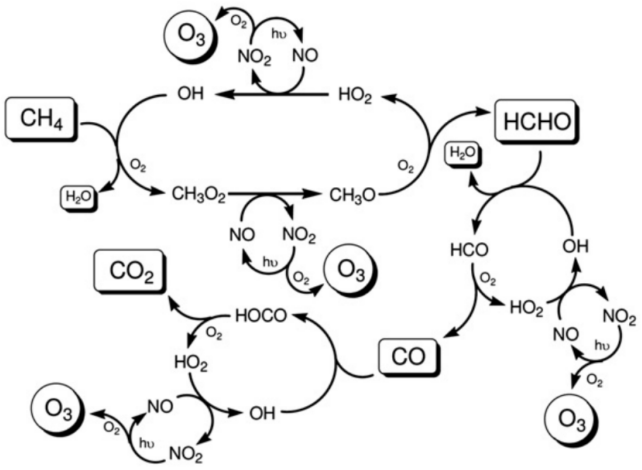

Figure 12. Schematic representation of the OH initiated, NO_x-catalysed oxidation scheme for CO and CH_4 [138].

6.1.3. NO_x-saturated regime

Under very high NO_x conditions, such as inside aircraft exhaust plumes or in regions of the atmosphere where aircraft fly in close proximity and their corresponding emissions accumulate, the ozone production efficiency starts to drop off. This is because as NO and NO_2 surpass a threshold concentration, known as the compensation point (peak of the curve in figure 14), they begin to compete with VOCs (e.g. methane) for reaction with hydroxyl (OH), organic peroxy (RO_2) and peroxide RCO_3 radicals [35]. The products of these reactions are examples of nitrogen reservoir species: nitrous acid (HONO), nitric acid (HNO_3), peroxynitric acid (HO_2NO_2), peroxy nitrates (RO_2NO_2) and peroxyacyl nitrates (RCO_3NO_2). Reservoir species are much less efficient at forming ozone as they are more stable and are also more likely to get washed out of the atmosphere through depositional processes [145]. They are also much more stable in the upper troposphere compared to the surface equivalent [150]. Thus, reactions (R19) to (R23) serve as termination reactions, removing radicals from the atmosphere and preventing additional ozone formation through conversion of NO_x to its more stable counterparts.

$$NO + OH + M \longrightarrow HONO + M \quad \text{(R19)}$$

$$NO_2 + OH + M \longrightarrow HNO_3 + M \quad \text{(R20)}$$

$$NO_2 + HO_2 + M \longrightarrow HO_2NO_2 + M \quad \text{(R21)}$$

$$NO_2 + RO_2 + M \longrightarrow RO_2NO_2 + M \quad \text{(R22)}$$

$$NO_2 + RCO_3 + M \longrightarrow RCO_3NO_2 + M \quad \text{(R23)}$$

NO_x saturation effects become particularly important to observe in the case of diluting aircraft exhaust plumes, because the high NO_X-VOC ratio means that termination reactions are often favoured over catalytic ozone formation [151]. In the relatively fresh exhaust plume (first 10 minutes) where NO_x concentrations are significantly enhanced, ozone titration by NO results in large scale production of NO_2 (R24), but decreases the formation of HO_x due to depleted ozone levels in the plume.

$$NO + O_3 \longrightarrow NO_2 + O_2 \quad \text{(R24)}$$

The dilution of the plume results in reduced NO_x concentrations over time, and the in-plume chemistry transitions from NO_x-saturated to NO_x-limited. With ozone levels still depleted, the remaining HO_2 and RO_2 in the plume (formed from the oxidation of CO and VOCs by OH) react with the remaining NO to produce OH and NO_2 without further depleting ozone. This leads to increasing OH and NO_2 concentrations which give rise to a net ozone recovery due to NO_2 photolysis (reactions (R11) and (R12)), with full recovery to ambient concentrations within 1–2 h post emission. As ozone levels rise in the plume back towards ambient concentrations, the photochemical formation of OH becomes more common, through reactions (R1) and (R2). Newly formed OH can oxidise CO and VOCs to form peroxy radicals which catalyse ozone production, however it can also react with NO and NO_2 to form stable nitrogen reservoir species, through reactions (R19) to (R23) [52].

In the ID scenario inherent to large-scale climate models, ozone titration doesn't occur on the same scale due to lower mixing ratios of NO_x when instantly diluted. Therefore, initial ozone depletion and subsequent recovery in the exhaust plume is not properly captured, meaning that instead, ozone levels remain reasonably high throughout and hence HO_x production can remain stable. The stable HO_x levels mean NO_x to reservoir species conversion remains stable also, throughout the NO_x lifetime. On a global scale, it has been shown that inclusion of plume processes leads to a net reduction in ozone forming potential of aviation NO_x emissions. Vohralik et al. (2008) [50] summarises the estimates made for the degree of reduction in ozone forming potential when plume effects were included. Initial findings from Kraabol et al. (2002) [152] and Meijer et al. (1997) [153] estimated discrepancies in ozone production of 15–18%, however these studies only accounted for ozone depletion in the plume, and not the O_3 generated during plume expansion. Inclusion of both ozone depletion and production in the plume in Meijer (2001) [53], led to updated estimated in ozone formation changes 0% to -5% in January and +5% to -10% in July, indicating that plume processing can actually increase net ozone production when propagated to global scales.

6.2. Heterogeneous chemistry

Reactions occurring in the atmosphere on either the gas–solid interface (e.g. aerosol particles) or the gas–liquid interface (e.g. cloud droplets) are referred to as heterogeneous reactions. The heterogeneous chemistry which can affect ozone concentrations through production and loss of HO_x and NO_x and the production of halogen radicals is extremely important in particle rich aircraft exhaust plumes and contrails [154]. The exhaust plume contains emitted soot particles and ultrafine aqueous aerosol particles which are either formed within the plume or entrained into the plume from ambient air, as elaborated on in the following subsection. In the case of contrail formation, heterogeneous chemistry becomes very efficient, due to the four-fold increase in particle surface area of contrail ice compared to typical exhaust and background aerosol surface area. Meilinger et al.

(2005) [155] states that the heterogeneous reactions occurring on aerosol particles have a negligible effect on ozone, however contrail ice can influence the ozone response to aircraft emissions by $\pm 0.5\%$ on a macroscopic scale which varies depending on time of day and year. Due to the relatively minor impact heterogeneous chemical reactions have on aircraft-induced ozone perturbations, and hence on aviation climate impact, their effect will be acknowledged, but the chemical intricacies will not be discussed further. For more information, see the references contained within this paragraph.

6.3. Aerosol and contrail microphysics

Whilst the climate impact of aviation NO_x emissions is dependent on the photochemical processes catalysing ozone production and methane destruction, the evolution and radiative forcing of aerosols and contrails is predominantly controlled by microphysical processes that occur at the aircraft plume scale.

6.3.1. The microphysical formation of aerosols and contrails

Upon release into the atmosphere, aerosol particle formation occurs through one of two nucleation pathways:

1. The condensation of two distinct gas phase molecules to form a liquid phase droplet through what is known as binary homogeneous nucleation. This is the case for reactive sulfur emissions that get chemically oxidised into sulphuric acid (H_2SO_4), which then condenses with water vapour to form H_2SO_4 / H_2O droplets [156].
2. The gas-to-particle conversion occurring on the surface of foreign particles is known as binary heterogeneous nucleation, often leading to a liquid coating that forms on the particle. For example, H_2SO_4 / H_2O droplets can form a partial liquid coating around chemically activated soot in the aircraft exhaust plume through heterogeneous nucleation, leading to soot aerosol formation; a process that plays an important role in the formation of contrails [157].

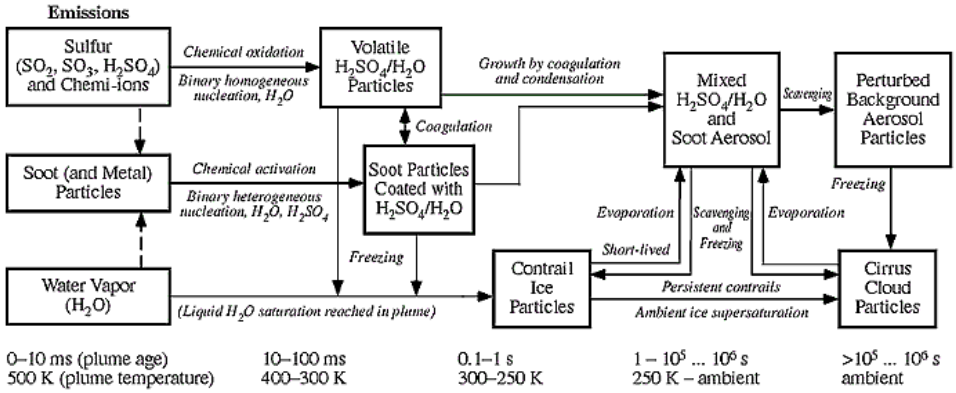

Figure 13. The microphysical formation of aerosol and contrail particles in an aircraft plume. Displayed as a function of plume age and temperature [14].

Newly formed aerosol particles subsequently grow in the aircraft wake due to further condensation by uptake of surrounding water vapour, and a process known as coagulation. Coagulation refers to the collision between particles that results in the formation of larger particles, often initiated by graviational settling, turbulence or thermal motion. A process called scavenging occurs when two particles, one much larger than the other, coagulate and lead to the removal of the small particle from its particular size category, with its mass contributing slightly to the increase in mass of the larger particle. Coagulation commonly occurs in aircraft wakes between volatile particles such as H_2SO_4 / H_2O particles and soot aerosol, forming a mixed H_2SO_4 / H_2O-soot aerosol (see figure 13. This sulphate-soot aerosol may eventually become scavenged by background aerosol particles if it remains stable for up to a day [14]. Alternatively, if at

any point during the mixing process of aircraft exhaust with air, water-supersaturation is exceeded, aircraft-induced particles and entrained background aerosol can be activated into water droplets through the uptake of surrounding water vapour [102]. If temperatures are below threshold according to the SA criterion, then these aerosol-activated water droplets will freeze to form contrail ice particles in the aircraft wake on the order of seconds post emission.

6.3.2. Contrail microphysical properties

The aforementioned microphysical processes (i.e. nucleation, condensation, coagulation, scavenging and freezing) determine the eventual composition and size distribution of particles in the aircraft wake, and if thermodynamic conditions permit, the formation and evolution of contrail ice particles [32,114]. Hereinafter, this section will focus on the microphysics of contrail ice particles, as they induce the most significant radiative response out of all aviation climate forcers. Findings from Kärcher et al. (1996b) [158] conclude that the predominant ice nucleation pathway for contrail formation is heterogeneous freezing of chemically activated soot aerosol particles, as these are the only remaining particle type in sufficient abundance at the time of freezing. However, simulation results from Kärcher et al. (1998) [84] strongly suggest that contrail formation is still likely in the absence of soot and sulphur emissions, through the activation and freezing of background aerosols.

The radiative forcing of contrails is thought to be determined by the product of optical depth and areal coverage [112]. In terms of areal coverage, contrail forcing is thus dominated by the presence of persistent contrails and contrail cirrus. However, the optical depth of a contrail is less dependent on its macroscopic properties and is instead determined by the optical and physical characteristics of the ice particles on the microscopic scale. The microphysical parameters deemed to be most responsible for inducing a radiative response are ice water content (amount of cloud ice per unit volume [102]), total ice particle number concentration, ice particle size distributions, effective radii, and ice particle shape [159]. Various studies have formulated methods to estimate RF and ERF from contrails, based on the parametrisation of these properties [160–162]. It is defined that the optical depth is proportional to the ice water content divided by the effective radius of entrained ice particles [161]. Contrails that tend to have more aspherical ice particle shapes are likely to have a stronger solar albedo, increasing the reflectance of the SW flux [160]. Ice number concentration is also thought to increase optical depth [163].

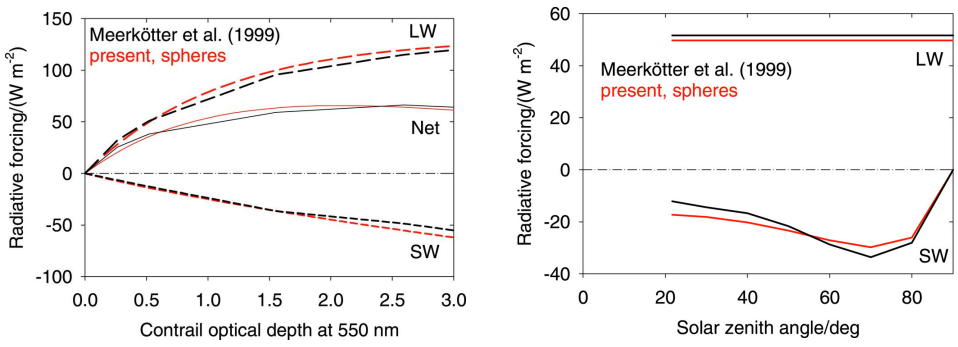

Figure 14. **(a)** Daily mean instantaneous SW, LW and net components of RF assuming 100% contrail cover vs optical depth as calculated using the spherical ice particle model from Schumann et al. (2012b) [164]. Results from Meerkötter et al. (1999) [160] shown for comparison. **(b)** RF vs SZA for spherical ice particles, with Meerkötter comparison shown. See Schumann et al. (2012b) [164] for more detail on assumed atmospheric conditions.

Optical depth of contrail cirrus is generally seen to increase radiative forcing, however the relationship is nonlinear and under assumed atmospheric conditions [160, 164], contrail RF increases with optical depth up to around 2.0, where it peaks, before decreasing at higher optical depths (see figure **??**). This is due to the lessening increase of positive LW forcing with increasing optical depth, whilst negative SW forcing continues to drop at a similar rate throughout. In addition to contrail optical properties, the magnitude and direction of contrail forcing is also directly determined by solar position, otherwise known as the solar zenith angle (SZA) (see figure **??**). Throughout the range of SZA values, LW forcing remains constant, because infrared emission from the Earth's surface is unaffected by solar flux. The SW flux on the other hand, goes further negative as SZA increases, up until a maximum at around 70°. Beyond this, the Sun begins to set and SW forcing returns to zero when the Sun is at 90° to the Earth's surface. This confirms the notion that contrails are solely warming at night, as the positive LW forcing always remains constant, whilst at night there is no chance of negative SW forcing.

6.4. The saturation of aircraft emissions in high-density airspace regions

In dense airspace regions, where the frequency of traversing aircraft is high, the resulting exhaust plumes may intersect and overlap, further affecting the nonlinear atmospheric response to chemical and microphysical processing occurring at the plume scale. Two outstanding saturation effects documented in the literature include the surpassing of NO_x-saturated conditions and the dehydration of surrounding water vapour due to contrail formation, leading to the mutual inhibition of ice particle growth in the aircraft wake.

6.4.1. NO_x-saturated conditions

The accumulation of nitrogen oxide emissions in the troposphere due to overlapping aircraft plumes has been observed empirically. For example, Schlager et al. (1997) [55] witnessed NO_x concentrations of up to 30 times the average background concentrations in the North Atlantic Flight Corridor, for an overlap of 2 to 5 aircraft plumes. The net ozone production rate in the upper troposphere is a nonlinear function of the concentrations of NO and NO_2, with increasing NO_x leading to increasing O_3, up until a maximum, where any additional NO_x serves to reduce ozone production efficiency (e.g. figure **??**). The turnover point, sometimes called the "compensation point" is determined by competitive reactions involving nitrogen species and HO_x. In the NO_x-limited regime (left of $P(O_3)_{max}$), NO drives the production of ozone through reaction with hydroperoxy radical (HO_2) [143]. However, it also drives the removal of HO_x through the reaction of OH with HO_2, HNO_4 and NO_2, thus limiting HO_x available for further O_3 production [165]. As NO_x levels increase up to compensation point, the increasing competition of HO_x removal processes begins to level off ozone production efficiency. Beyond this point, further increases in NO_x serve to decrease $P(O_3)$, thus signalling the start of the NO_x-saturated regime.

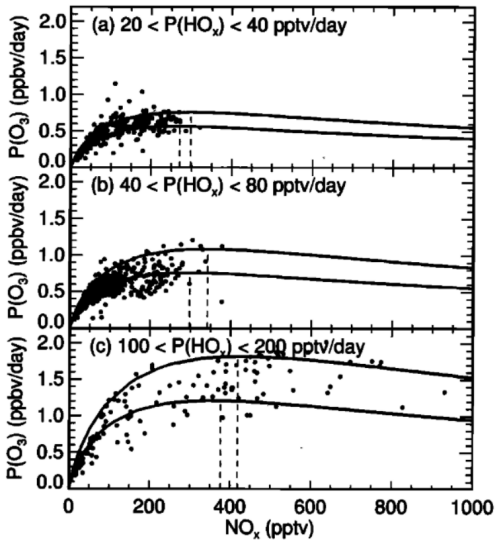

Figure 15. Empirical observations of ozone production rate as a function of NO_x concentrations (parts per trillion volume), for three ranges of primary HO_x production: (a) 20–40 pptv/day, (b) 40–80 pptv/day, and (c) 100–200 pptv/day. Solid lines represent the range limits from model calculations. Dashed lines depict the NO_x level that induces peak ozone response [5].

During the POLINAT/SONEX campaign, Jaeglé et al. (1999) [5] presents the first empirical evidence of NO_x-saturated conditions in the NAFC. As seen in figure 15 at 100–200 pptv/day of HO_x production, $P(O_3)$ levels increased with increasing NO_x up until around 300 pptv, where it is clear that NO_x saturation has been reached. This means that any further emission of NO_x under those specific atmospheric conditions will potentially serve to decrease the net ozone production rate. Generally speaking, ozone production efficiency, and hence the threshold for NO_x-saturated conditions, is largely dependent on just two variables: the ambient NO_x concentration (including the accumulation of NO_x from lingering aircraft plumes) and the HO_x production rate (which depends on the chemical composition of the atmosphere and the solar intensity [143]) [166].

Furthermore, model results from Kraabol et al. (2000b) [115] in a study observing interactions between plumes revealed that, for aircraft flying along the same track, plumes of follower aircraft exhibit a considerably smaller ozone response than that of the leader aircraft. This observation on a local scale opens up the discussion for controlled saturation of emissions through formation flight, to take advantage of effects that are beneficial to the climate.

6.4.2. Dehydration effects due to contrail formation

Contrails grow and persist in the atmosphere through deposition of water vapour from ice-supersaturated layers of the atmosphere. The conversion of atmospheric water vapour to solid phase ice particles has the potential to deplete local water vapour concentrations in regions conducive to persistent contrail generation [167]. It is thought that the depositional growth of contrail cirrus in regions of high airspace density can even lead to the dehydration of H_2O at typical flight levels, followed by the redistribution of humidity to lower levels, due to sedimentation and advection processes [6].

Contrail dehydration effects were first quantified by Burkhardt and Kärcher (2011) [100], in which a global atmospheric model was used to perform long-term integrations of the global impact of contrail cirrus on natural cirrus reduction due to ambient water vapour depletion. The paper found initial RF estimates to be -7 mWm^{-2}, lessening the contrail cirrus RF estimate by a factor of approximately one fifth, however the results were not conclusive. Schumann et al. (2015) [6] furthered this investigation through quantification of the impact of water exchange on contrail properties, large-

scale humidity and the background climate. The results suggested that the drying at flight levels caused contrails to become thinner and last longer in the atmosphere, and the net reduction in contrail cirrus RF was deemed to be ~15% (not too dissimilar to the results of the Burkhardt and Kärcher (2011) [100]). Furthermore, the results from a second run of the model, with aircraft emissions enhanced by 100 times, showing increasingly significant dehydration effects due to contrail cirrus formation and the redirection of humidity to lower flight levels. This implies that local dehydration effects will be far more significant in dense airspace regions where emissions accumulate and contrails can overlap, such as over mainland areas and in flight corridors. Work by Unterstrasser [167,168] has elaborated on this concept of local dehydration, through numerical analysis of contrail growth in close proximity flight scenarios. The studies conclude that aircraft contrails compete for available water vapour, mutually inhibiting growth and leading to a saturation effect which diminishes the contrail of subsequent aircraft travelling through that region. Under proposed formation flight scenarios, the total extinction (optical depth) and total ice mass behind a two-aircraft formation are found to be reduced by 20–50% and 30–60% respectively.

The presence of plume-scale effects that are amplified in close-proximity flight scenarios begs the question; can climate beneficial saturation effects such as NO_x-saturated regimes and contrail-induced dehydration be exploited for mitigation purposes? Section 7 explores the concept of formation flight and how these additional climate benefits from emissions saturation may provide further impetus for real-world implementation of these concepts.

6.5. Parametrisation of plume-scale effects into global models

Plume modelling methods serve as a useful tool for analysing the chemical and physical evolution of aircraft exhaust plumes throughout their lifetime. However, integrating high-resolution plume data into global atmospheric models is simply unfeasible when a large number of flights, on the order of 100,000–200,000 flights per day [169], must be considered. To counteract this, simpler parametrisations of plume models are used, which capture so-called “effective emissions" that attempt to correct the ID response of the large-scale model, according to the predicted plume-scale effects and their influence on the eventual climate impact. Parametrising plume-scale climate effects into global atmospheric models that assume instantaneous dispersion is a topic covered extensively in the literature, for both ozone-NO_x chemistry [4,39,153,170] and contrail and cloud processes [171].

6.5.1. Parametrisation of gas-phase chemical conversions

In Paoli et al. (2011) [4], three key concepts are reviewed which enable the parametrisation of nonlinear plume chemistry into ID global models; effective emission indices (EEIs), effective conversion factors (ECFs) and effective reaction rates (ERRs).

The EEI concept was first theorised in Petry et al. (1998) [38], in an attempt to account for the difference in concentration evolution of key chemical species between large scale models which assume ID and plume models which account for the entrainment of emissions throughout the plume lifetime. EEIs provide a suitable correction to the original EI of an emitted species, so that the concentration is the same in both models at the end of the plume “dispersion time" t_{ref}, when emissions are fully dispersed into the dimensions of the computational grid cell in which they were released.

Meijer (2001) [53] presents the concept of ECFs which are factors applied to the NO_x emission index to account for the increased chemical conversion rate of NO_x to nitrogen reservoir species in the plume. Since the total emitted reactive nitrogen (NO_y) is chemically conserved throughout the plume lifetime, the amount of NO_y throughout the plume lifetime is equal to the amount of NO_x emitted initially, and hence the sum of ECFs for NO_x and all reservoir species is unity [50]. Thus, the faster in-plume conversion rates lead to a decreased NO_x ECF, whilst the ECFs of reservoir species such as HNO_2

and HNO_3 increase considerably. As a result, the eventual net ozone production is affected as explained in section 6.1, however ECFs vary considerably depending on altitude, latitude and seasonal variation meaning the magnitude and direction of the ozone perturbation is also affected.

Despite the widespread use of EEIs and ECFs to parametrise plume-scale gas-phase chemical conversions in past literature, there are a number of known issues that affect accuracy such as mass conservation inconsistencies and poor accounting of local and regional variation in dispersion properties and turbulence. Cariolle et al. (2009) [39] attempts to overcome such issues with the ERR concept. ERRs reconstruct the concentrations of the emitted species in the plume by diluting the emission to the resolution of the computational grids cell, while modified reaction rates are used to model reactions with ambient chemical species that occur at the plume scale. Modified reaction rates are introduced by the determination of effective reaction rate constants, which are used to compute secondary species produced in the plume. As a result, ERRs build on the EEI and ECF concepts by ensuring full mass conservation by modulating pre-existing background chemical cycles instead of directly estimating mass change, and they account for chemical transport due to diffusion and turbulence processes that are entirely dependent on location.

6.5.2. Parametrisation of heterogeneous chemistry and microphysics

Despite there being an extensive number of gas-phase chemistry parametrisations, the same cannot be said for parametrisations of heterogeneous chemistry and microphysics, for modelling aircraft plume-scale climate effects at a global scale. Kärcher et al. (1998) [84] was one of the first studies to explicitly attempt to parametrise heterogeneous reactions and aerosol microphysics in global models. The paper attributed the perturbations to the background aerosol layer (due to aerosol emissions from aircraft) to increasing surface areas and number concentrations of aerosol particles, which subsequently increase heterogeneous reaction rates. Findings from Meilinger et al. [155,172] however, reveal that heterogeneous chemistry effects in dispersing aircraft plumes require special consideration of both the chemical and microphysical interactions, and the dynamical response of the plume itself. In Meilinger et al. (2005) [155], the Mainz Aircraft Plume Model is used to calculate the response of ozone and nitrogen reservoir species in the plume due to heterogeneous chemistry and microphysical effects. It is found from the modelling results that the impact of heterogeneous chemistry and microphysics on the ozone response at global scales is highly sensitive to local meteorology and the instantaneous state of the atmosphere. Therefore, parametrisation of these effects is much more convoluted than first thought, and due to the relatively minute impact on ozone response ($\pm$0.5%), it is not unreasonable to disregard these effects in global modelling efforts.

Contrarily, the parametrisation of contrail microphysics into global models is of crucial importance, as contrail radiative forcing is determined primarily by the optical properties of its consituent ice particles. Burkhardt and Kärcher (2009) [171] summarise the parametrisations necessary to include contrail radiative forcing in global models; this includes parametrising the factors affecting ice supersaturation, contrail formation and persistence, contrail spreading and ice water content. This led to the development of the process-based contrail cirrus module (CCMod), which was later implemented in the global climate model ECHAM4, for global contrail cirrus radiative forcing analysis [100,173,174]. More recently, a microphysical extension to CCMod was applied and implemented in ECHAM5 [162,175]. Model outputs were used to determine the global effective radiative forcing of contrail cirrus in Lee et al. (2021) [1], finding that the ERF is more than 50% smaller than the RF equivalent. This is thought to be due to the reduction in natural cloudiness caused by contrail cirrus dehydration of the surrounding atmosphere, and due to the dependence of contrail climate impact on prevailing air

traffic distribution patterns. See Lee et al. (2021) [1] for more info on the parametrisations of contrail and aerosol microphysics implemented to deduce global ERF estimates.

7. Aviation climate impact mitigation

It is customary practice among aviation policymakers to solely focus on mitigating the greenhouse effect induced by aviation carbon emissions. This means that analysis of the climate impact of non-CO_2 emissions is largely neglected, despite being responsible for the majority of aviation-induced climate change.

7.1. CO_2 mitigation

The industry fixation on aviation CO_2 mitigation stems from the easily quantifiable nature of the substance and its impacts; the direct coupling to fuel consumption and its relative stability and long lifetime make it a prime target for mitigation. This is due to the assured reduction in both fuel consumption and corresponding CO_2 emissions, providing an economic and environmental incentive. Conventional mitigation approaches have often taken the form of improvements to aircraft and engine design, aviation technology and infrastructure, and aircraft operations, all aimed at minimising aircraft fuel consumption. These changes have been largely incremental due to the prioritisation of safety and economic stability over rapid implementation. As a result, efficiency gains have stalled in recent years (1–2% per annum), whilst growth rates continue to increase significantly (4–5% per annum) [1**?**].

Alternatively, the industry has looked towards longer term mass mitigation measures such as the implementation of sustainable aviation fuels (SAFs) and zero carbon propulsion concepts such as hydrogen- or electric-powered flight. SAFs are renewable or waste-derived fuels that meet specific sustainability criteria laid out in ICAO Annex 16 Vol. IV [**?**]. These fuels typically have lower life-cycle CO_2 emissions of up to 80% [], and also reduced PM emissions of soot and sulphate by 28–98% depending on a range of SAF fuel types [**?**].

7.2. Non-CO_2 mitigation

As alluded to in sections **??** and **??**, non-CO_2 emissions are on the other hand, produced in varying quantities depending on combustor conditions. Also, when released into the atmosphere, they have a spatio-temporally sensitive climate response, depending on the background atmospheric conditions into which they are emitted. As such, anthropogenic as well as natural perturbations to atmospheric chemistry need to be considered; the entrainment of emissions to the exhaust plume for several hours post emission, leads to locally elevated emissions concentrations. This causes reactive non-CO2 species to experience nonlinear chemical and microphysical processing that occurs at the scale of the plume, which subsequently affects their net climatic response when propagated to global scales [].

Mitigation of non-CO2 climate impact therefore requires an optimisation of the atmospheric conditions in which aircraft emissions are released, which can be achieved through two noteworthy operational mitigation procedures, climate-optimal aircraft routing and formation flight.

The first of these is climate-optimal aircraft routing. This involves re-routing aircraft in flight to avoid regions of the atmosphere that are particularly sensitive to non-CO2 climatic effects, such as where NOx gives rise to excessive ozone production or where persistent contrails are formed [10]. Simulation efforts have suggested that this method has the potential to reduce aviation climate impact by 10-20%, at the cost of only a few percent of additional fuel consumption [11, 12].

This section explores the potential for adjustments to aircraft operations that can be implemented, in the interest of mitigating aviation climate impact.

These mitigation which utilise knowledge of the spatio-temporal variability in the atmospheric response to aircraft emissions,

Mention alt fuels, alt propulsion, technological changes etc. and say how they are long term due to infrastructure overhaul and large investment. Operational mitigation strategies require minimal change to current system, only operational changes which can be implemented without much additional investment. Just need more research and

7.2.1. Formation flight

Formation flight involves the flight of two or more aircraft in aerodynamic formation, with the follower aircraft positioned in the smooth updraft of the leader aircraft's wake, reducing required lift and thrust, hence reducing fuel and CO2 emissions by 5-8% per trip 14. A fortuitous outcome of formation flight is however, the saturation of emissions in the trailing exhaust plumes, which can lead to the aforementioned nonlinear chemical and microphysical response that reduces ozone and contrail formation. The non-CO2 climate effects of a twin-aircraft formation flight are observed in 14, where a climate model was used to determine the changes in NOx-related ozone production and contrail formation processes. The case study found that, despite a 1-3% increase in flown distance, CO2 was reduced by 6% and NOx was reduced by 11%. This resulted in a 5% reduction in ozone production efficiency due to NOx saturation and a 48% contrail reduction due to mutual competition for available water vapour, resulting in a total climate impact reduction of approximately 23%. While part of the alleviated climate impact can be related to the decrease in total emissions due to wake energy retrieval of the follower aircraft, there is also further emphasis due to the saturation of emissions in the overlapping plumes of both aircraft involved. This demonstrates great potential for reducing both CO2- and non-CO2-induced climate effects from aviation, if such a scheme were to be carried out on a global scale.

7.2.2. Climate-optimal aircraft routing

Fleet-wide implementation of formation flight would however, pose a number of research obstacles, that must be overcome to maximise its cost-benefit potential, whilst ensuring the safe and orderly operation of aircraft in controlled airspace. Optimising aircraft trajectories to minimise fuel burn requires the consideration of nonlinear aircraft performance, wind and weather, payload, fuel load, and constraints set out by air traffic control []. Formation flight adds another variable to the fuel burn optimisation problem, maximising the time spent flying in formation whilst minimising deviation from the true optimal route. This is a research topic covered extensively in the literature []. Optimising formation flight trajectories to minimise climate impact on the other hand, is a relatively novel concept, which requires deeper understanding of the sensitivity of the climate response to emissions under a range of different atmospheric states.

Newinger and Burkhardt (2012) [113] explored the potential for mitigation of nighttime contrail forcing through air traffic scheduling adjustments. They proposed...

Teoh et al. investigated the possibility of small-scale diversion of aircraft to avoid persistent contrail formation in most sensitive regions and achieved a ... reduction in contrail climate impact for a ... increase in ... .

8. Conclusions

> Maximum ozone depletion in c

1. Lee, D.; Fahey, D.; Skowron, A.; Allen, M.; Burkhardt, U.; Chen, Q.; Doherty, S.; Freeman, S.; Forster, P.; Fuglestvedt, J.; Gettelman, A.; De León, R.; Lim, L.; Lund, M.; Millar, R.; Owen, B.; Penner, J.; Pitari, G.; Prather, M.; Sausen, R.; Wilcox, L. The contribution of global aviation to anthropogenic climate forcing for 2000 to 2018. *Atmospheric Environment* **2021**, *244*, 117834. doi:10.1016/j.atmosenv.2020.117834.
2. Kraabøl, A.G.; Konopka, P.; Stordal, F.; Schlager, H. Modelling chemistry in aircraft plumes 1: Comparison with observations and evaluation of a layered approach. *Atmospheric Environment* **2000**, *34*, 3939–3950. doi:10.1016/S1352-2310(00)00156-4.

3. Workbook for plume visual impact screening and analysis (revised). Technical report, United States Environmental Protection Agency (EPA), 1992.
4. Paoli, R.; Cariolle, D.; Sausen, R. Review of effective emissions modeling and computation. *Geoscientific Model Development* **2011**, *4*, 643–667. doi:10.5194/gmd-4-643-2011.
5. Jaeglé, L.; Jacob, D.J.; Brune, W.H.; Faloona, I.C.; Tan, D.; Kondo, Y.; Sachse, G.W.; Anderson, B.; Gregory, G.L.; Vay, S.; Singh, H.B.; Blake, D.R.; Shetter, R. Ozone production in the upper troposphere and the influence of aircraft during SONEX: approach of NO_x-saturated conditions. *Geophysical Research Letters* **1999**, *26*, 3081–3084. doi:10.1029/1999GL900451.
6. Schumann, U.; Penner, J.E.; Chen, Y.; Zhou, C.; Graf, K. Dehydration effects from contrails in a coupled contrail–climate model. *Atmospheric Chemistry and Physics* **2015**, *15*, 11179–11199. doi:10.5194/acp-15-11179-2015.
7. Niklaß, M.; Lührs, B.; Grewe, V.; Dahlmann, K.; Luchkova, T.; Linke, F.; Gollnick, V. Potential to reduce the climate impact of aviation by climate restricted airspaces. *Transport Policy* **2019**. doi:10.1016/j.tranpol.2016.12.010.
8. Bangash, Z.A.; Sanchez, R.P.; Ahmed, A.; Khan, M.J. Aerodynamics of formation flight. *AIAA Paper* **2004**, pp. 8399–8408. doi:10.2514/6.2004-725.
9. Kent, T.E.; Richards, A.G. Potential of Formation Flight for Commercial Aviation: Three Case Studies. *Journal of Aircraft* **2020**, *58*, 320–333. doi:10.2514/1.C035954.
10. Dahlmann, K.; Matthes, S.; Yamashita, H.; Unterstrasser, S.; Grewe, V.; Marks, T. Assessing the climate impact of formation flights. *Aerospace* **2020**, *7*, 1–12. doi: 10.3390/aerospace7120172.
11. Gössling, S.; Humpe, A. The global scale, distribution and growth of aviation: Implications for climate change. *Global Environmental Change* **2020**, *65*. doi: 10.1016/j.gloenvcha.2020.102194.
12. Hemighaus, G.; Boval, T.; Bacha, J.; Barnes, F.; Franklin, M.; Gibbs, L.; Hogue, N.; Jones, J.; Lesnini, D.; Lind, J.; Morris, J. Aviation Fuels Technical Review. Technical report, Chevron U.S.A, 2007. doi:10.1097/RLU.0000000000001475.
13. Holladay, J.; Abdullah, Z.; Heyne, J. Sustainable Aviation Fuel: Review of Technical Pathways. Technical report, U.S Department of Energy, 2020.
14. Penner, J.; Lister, D.; Griggs, D.; Dokken, D.; McFarland, M., Aviation and the Global Atmosphere; Cambridge University Press, 1999; chapter 2.
15. Celikel, A.; Jelinek, F. Forecasting Civil Aviation Fuel Burn and Emissions in Europe. Technical report, EUROCONTROL Experimental Centre, 2001.
16. Brasseur, G.; Cox, R.; Hauglustaine, D.; Isaksen, I.; Lelieveld, J.; Lister, D.; Sausen, R.; Schumann, U.; Wahner, A.; Wiesen, P. European scientific assessment of the atmospheric effects of aircraft emissions. *Atmospheric Environment* **1998**, *32*, 2329–2418. doi: 10.1016/S1352-2310(97)00486-X.
17. Deidewig, F.; Dopelheuer, A.; Lecht, M. Methods to Assess Aircraft Engine Emissions in Flight. Technical report, 1996.
18. Döpelheuer, A. Aircraft emission parameter modelling. *Air & Space Europe* **2000**, *2*, 34–37. doi:10.1016/S1290-0958(00)80060-X.
19. Dopelheuer, A.; Lecht, M. Influence of engine performance on emission characteristics. *RTO-Symposium of AVT on Gas Turbine Engine Combustion, Emissions and Alternative Fuels* **1998**.
20. Gettelman, A.; Chen, C. The climate impact of aviation aerosols. *Geophysical Research Letters* **2013**, *40*, 2785–2789. doi:10.1002/grl.50520.
21. Aircraft fuels and their effect upon engine emissions. *Air & Space Europe* **2001**, *3*, 101–103. doi:10.1016/s1290-0958(01)90026-7.
22. Bockhorn, H., Soot Formation in Combustion; Springer, Berlin, Heidelberg, 1994.
23. Wayson, R.L.; Fleming, G.G.; Iovinelli, R.; Wayson, R.L.; Fleming, G.G.; Iovinelli, R.; Wayson, R.L.; Fleming, G.G. Methodology to Estimate Particulate Matter Emissions from Certified Commercial Aircraft Engines Methodology to Estimate Particulate Matter Emissions from Certified Commercial Aircraft Engines **2012**. *2247*. doi:10.3155/1047-3289.59.1.91.
24. Schumann, U.; Arnold, F.; Busen, R.; Curtius, J.; Ka, B.; Kiendler, A.; Petzold, A.; Wohlfrom, K. Influence of fuel sulfur on the composition of aircraft exhaust plumes : The experiments SULFUR 1 – 7 **2002**. *107*.
25. Masiol, M.; Harrison, R.M. Aircraft engine exhaust emissions and other airport-related contributions to ambient air pollution : A review Aircraft Particle Emissions eXperiment. *Atmospheric Environment* **2014**, *95*, 409–455. doi:10.1016/j.atmosenv.2014.05.070.

26. Nuic, A.; Poles, D.; Mouillet, V. BADA: An advanced aircraft performance model for present and future ATM systems. *International Journal of Adaptive Control and Signal Processing* **2010**, *24*, 850–866. doi:10.1002/acs.1176.
27. Piano-X Aircraft Emissions and Performance User's Guide. Technical report, Lissys Ltd, 2008.
28. Aviation Environment Design Tool (AEDT) 2a: Technical Manual, Version 3c. Technical report, Federal Aviation Administration (FAA), 2020.
29. Sun, J.; Hoekstra, J.M.; Ellerbroek, J. OpenAP: An Open-Source Aircraft Performance Model for Air Transportation Studies and Simulations. *Aerospace* **2020**, *7*, 104. doi: 10.3390/aerospace7080104.
30. International Civil Aviation Organization (ICAO) Committee on Aviation Environmental Protection (CAEP). *ICAO Aircraft Engine Emissions Databank*, 28 ed.; 2021.
31. International Civil Aviation Organization (ICAO). Annex 16 to the Convention on International Civil Aviation–Volume I–Aircraft Noise. *Icao* **2008**, *552*.
32. SAE Aerospace. *Procedure for the Calculation of Aircraft Emissions*, 2009. doi: https://doi.org/10.4271/AIR5715.
33. Brink, L. Modeling the Impact of Fuel Composition on Aircraft Engine NOx, CO and Soot Emissions. Master's thesis, Massachusetts Institute of Technology, 2020.
34. DuBois, D.; Paynter, G.C. "Fuel Flow Method2" for Estimating Aircraft Emissions. SAE Technical Papers, 2006, Vol. 115, pp. 1–14. doi:10.4271/2006-01-1987.
35. Wasiuk, D.K. Modelling aircraft emissions and their impact on atmospheric composition and ozone. PhD thesis, University of Bristol, 2014.
36. Wasiuk, D.K.; Khan, A.H.; Shallcross, D.E.; Lowenberg, M.H. A Commercial Aircraft Fuel Burn and Emissions **2016**. *7*, 78. doi:10.3390/atmos7060078.
37. Mark Z. Jacobson. *Fundamentals of Atmospheric Modeling*, 2nd ed.; Cambridge University Press, 2005; [arXiv:1011.1669v3].
38. Petry, H.; Hendricks, J.; Möllhoff, M.; Lippert, E.; Meier, A.; Ebel, A.; Sausen, R. Chemical conversion of subsonic aircraft emissions in the dispersing plume: Calculation of effective emission indices. *Journal of Geophysical Research: Atmospheres* **1998**, *103*, 5759–5772. doi: 10.1029/97JD03749.
39. Cariolle, D.; Caro, D.; Paoli, R.; Hauglustaine, D.A.; Cuénot, B.; Cozic, A.; Paugam, R. Parameterization of plume chemistry into large-scale atmospheric models: Application to aircraft NOx emissions. *Journal of Geophysical Research Atmospheres* **2009**, *114*, 1–21. doi: 10.1029/2009JD011873.
40. Danilin, M.Y.; Ebel, A.; Elbern, H.; Petry, H. Evolution of the concentrations of trace species in an aircraft plume: trajectory study. *Journal of Geophysical Research* **1994**, *99*. doi: 10.1029/94jd01820.
41. Paoli, R.; Shariff, K. Contrail Modeling and Simulation. *Annual Review of Fluid Mechanics* **2016**, *48*, 393–427. doi:10.1146/annurev-fluid-010814-013619.
42. Gerz, T.; Dürbeck, T.; Konopka, P. Transport and effective diffusion of aircraft emissions. *Journal of Geophysical Research Atmospheres* **1998**, *103*, 25905–25913. doi:10.1029/98JD02282.
43. Crow, S.C. Stability Theory for a Pair of Trailing Vortices. *AIAA Journal* **1970**, *8*, 2172–2179. doi:10.2514/3.6083.
44. Unterstrasser, S.; Paoli, R.; Sölch, I.; Kühnlein, C.; Gerz, T. Dimension of aircraft exhaust plumes at cruise conditions: Effect of wake vortices. *Atmospheric Chemistry and Physics* **2014**, *14*, 2713–2733. doi:10.5194/acp-14-2713-2014.
45. Schumann, U.; Konopka, P.; Baumann, R.; Busen, R.; Gerz, T.; Schlager, H.; Schulte, P.; Volkert, H. Estimate of diffusion parameters of aircraft exhaust plumes near the tropopause from nitric oxide and turbulence measurements. *Journal of Geophysical Research* **1995**, *100*, 14147–14162.
46. Schumann, U.; Schlager, H.; Arnold, F.; Baumann, R.; Haschberger, P.; Klemm, O. Dilution of aircraft exhaust plumes at cruise altitudes. *Atmospheric Environment* **1998**, *32*, 3097–3103. doi: 10.1016/S1352-2310(97)00455-X.
47. Gerz, T.; Ehret, T. Wingtip Vortices and Exhaust Jets during the Jet Regime of Aircraft Wakes. *Aerospace Science and Technology* **1997**, *1*, 463–474. doi:10.1016/S1270-9638(97)90008-0.
48. Dürbeck, T.; Gerz, T. Dispersion of aircraft exhausts in the free atmosphere. *Journal of Geophysical Research Atmospheres* **1996**, *101*, 26007–26015. doi:10.1029/96jd02217.
49. Konopka, P. Analytical Gaussian Solutions for Anisotropie Diffusion in a Linear Shear Flow. *Journal of Non-Equilibrium Thermodynamics* **1995**, *20*. doi:10.1515/jnet.1995.20.1.78.

50. Vohralik, P.F.; Randeniya, L.K.; Plumb, I.C.; Baughcum, S.L. Effect of plume processes on aircraft impact. *Journal of Geophysical Research Atmospheres* **2008**, *113*, 1–21. doi: 10.1029/2007JD008982.
51. Dürbeck, T.; Gerz, T. Large-eddy simulation of aircraft exhaust plumes in the free atmosphere: Effective diffusivities and cross-sections. *Geophysical Research Letters* **1995**, *22*, 3203–3206. doi:10.1029/95GL03021.
52. Fritz, T.M.; Eastham, S.D.; Speth, R.L.; Barrett, S.R. The role of plume-scale processes in long-term impacts of aircraft emissions. *Atmospheric Chemistry and Physics* **2020**, *20*, 5697–5727. doi:10.5194/acp-20-5697-2020.
53. Meijer, E. Modelling the impact of subsonic aviation on the composition of the atmosphere. PhD thesis, Applied Physics, 2001. doi:10.6100/IR550468.
54. Melo, O.T.; Lusis, M.A.; Stevens, R.D.S. *Atmospheric Environment* **1978**, *12*, 1231–1234.
55. Schlager, H.; Konopka, P.; Schulte, P.; Schumann, U.; Ziereis, H.; Arnold, F.; Klemm, M.; Hagen, D.E.; Whitefield, P.D.; Ovarlez, J. In situ observations of air traffic emission signatures in the North Atlantic flight corridor. *Journal of Geophysical Research* **1997**, *102*, 10739–10750. doi:10.1029/96JD03748.
56. Fritz, T.M. Micro-Physical Modeling of Aircraft Exhaust Plumes and Condensation Trails. Master's thesis, Massachusetts Institute of Technology, 2018.
57. Fritz, T.M. personal communication.
58. Lewellen, D.C.; Lewellen, W.S.; Poole, L.R.; DeCoursey, R.J.; Hansen, G.M.; Hostetler, C.A.; Kent, G.S. Large-eddy simulations and lidar measurements of vortex-pair breakup in aircraft wakes. *AIAA Journal* **1998**, *36*, 1439–1445. doi:10.2514/2.535.
59. Paoli, R. Large-eddy simulation of a turbulent jet and a vortex sheet interaction : particle formation and evolution in the near field of an aircraft wake **2008**. doi: 10.1127/0941-2948/2008/0278.
60. Secretariat General. *Annex 11 Environment*; Number July, 2016; p. 18.
61. Zhang, W.; Kamgarpour, M.; Sun, D.; Tomlin, C.J. A hierarchical flight planning framework for air traffic management. *Proceedings of the IEEE* **2012**, *100*, 179–194. doi: 10.1109/JPROC.2011.2161243.
62. Baumgartner, M.; Cook, A.; Dennis, N.; Houtte, B.V.; Majumdar, A.; Pilon, N.; Tanner, G.; Williams, V. European Air Traffic Management: Principles, Practice and Research **2007**. p. 255.
63. Mitchell, J.S.; Polishchuk, V.; Krozel, J. Airspace throughput analysis considering stochastic weather. *Collection of Technical Papers - AIAA Guidance, Navigation, and Control Conference 2006* **2006**, *8*, 5070–5088. doi:10.2514/6.2006-6770.
64. Krozel, J.; Mitchell, J.S.; Polishchuk, V.; Prete, J. Capacity estimation for airspaces with convective weather constraints. *Collection of Technical Papers - AIAA Guidance, Navigation, and Control Conference 2007* **2007**, *2*, 1518–1532. doi:10.2514/6.2007-6451.
65. Federal Aviation Administration. FAQ: Weather Delay, 2021.
66. International Civil Aviation Authority. *Doc 4444 - Air Traffic Management - Procedures for Air Navigation Services*, 16 ed.; 2016.
67. The Flow Management Problem in Air Traffic Control. In *Flow control of congested networks*; Springer-Verlag Berlin Heidelberg, 1987; Vol. 38, pp. 269–288.
68. Bilimoria, K.D.; Sridhar, B.; Chatterji, G.B. Effects of conflict resolution maneuvers and traffic density on free flight. *1996 Guidance, Navigation, and Control Conference and Exhibit* **1996**, pp. 1–12. doi:10.2514/6.1996-3767.
69. Federal Aviation Administration., Instrument Procedures Handbook (IPH); 2017; chapter 2. En Route Operations.
70. Soler, M.; Olivares, A.; Staffetti, E. Multiphase optimal control framework for commercial aircraft four-dimensional flight-planning problems. *Journal of Aircraft* **2015**, *52*, 274–286. doi: 10.2514/1.C032697.
71. Altus, S. Effective Flight Plans Can Help Airlines Economize. https://www.boeing.com/commercial/aeromagazine/articles/qtr_03_09/pdfs/AERO_Q309_article08.pdf.
72. Murrieta-Mendoza, A.; Botez, R. Lateral navigation optimization considering winds and temperatures for fixed altitude cruise using Dijsktra's algorithm. *ASME International Mechanical Engineering Congress and Exposition, Proceedings (IMECE)* **2014**, *1*, 1–9. doi: 10.1115/IMECE2014-37570.
73. Ng, H.K.; Sridhar, B.; Grabbe, S. A practical approach for optimizing aircraft trajectories in winds. 2012 IEEE/AIAA 31st Digital Avionics Systems Conference (DASC). IEEE, 2012.

74. Majumdar, A.; Ochieng, W.Y.; McAuley, G.; Lenzi, J.M.; Lepadatu, C. The factors affecting airspace capacity in Europe: A cross-sectional time-series analysis using simulated controller workload data. *Journal of Navigation* **2004**, *57*, 385–405. doi:10.1017/S0373463304002863.
75. Welch, J.D.; Andrews, J.W.; Martin, B.D.; Sridhar, B. Macroscopic workload model for estimating en route sector capacity. *Proceedings of the 7th USA/Europe Air Traffic Management Research and Development Seminar, ATM 2007* **2007**, pp. 94–103.
76. Andrews, J.W.; Welch, J.D. 1st USA/EUROCONTROL ATM Seminar, Saclay, France, 1997.
77. Gardi, A.; Sabatini, R.; Ramasamy, S. Multi-objective optimisation of aircraft flight trajectories in the ATM and avionics context. *Progress in Aerospace Sciences* **2016**, *83*, 1–36. doi:10.1016/j.paerosci.2015.11.006.
78. Olsen, S.C.; Wuebbles, D.J.; Owen, B. Comparison of global 3-D aviation emissions datasets. *Atmospheric Chemistry and Physics* **2013**, *13*, 429–441. doi:10.5194/acp-13-429-2013.
79. Houghton, J.; Ding, Y.; Griggs, D.; Noguer, M.; van der Linden, P.; Dai, X.; Maskell, M.; Johnson, C., Climate Change 2001: The Scientific Basis; Cambridge University Press, 2001; chapter 1: The Climate System: an Overview, pp. 87–98.
80. Inness, A.; Baier, F.; Benedetti, A.; Bouarar, I.; Chabrillat, S.; Clark, H.; Clerbaux, C.; Coheur, P.; Engelen, R.J.; Errera, Q.; Flemming, J.; George, M.; Granier, C.; Hadji-Lazaro, J.; Huijnen, V.; Hurtmans, D.; Jones, L.; Kaiser, J.W.; Kapsomenakis, J.; Lefever, K.; Leitão, J.; Razinger, M.; Richter, A.; Schultz, M.G.; Simmons, A.J.; Suttie, M.; Stein, O.; Thépaut, J.N.; Thouret, V.; Vrekoussis, M.; Zerefos, C. The MACC reanalysis: An 8 yr data set of atmospheric composition **2013**. *13*, 4073–4109. doi:10.5194/acp-13-4073-2013.
81. Emmons, L.K.; Hauglustaine, D.A.; Müller, J.F.; Carroll, M.A.; Brasseur, G.P.; Brunner, D.; Staehelin, J.; Thouret, V.; Marenco, A. Data composites of airborne observations of tropospheric ozone and its precursors. *Journal of Geophysical Research: Atmospheres* **2000**, *105*, 20497–20538. doi:10.1029/2000JD900232.
82. Schanz, A.; Hocke, K.; Kämpfer, N.; Chabrillat, S.; Inness, A.; Palm, M.; Notholt, J.; Boyd, I.; Parrish, A.; Kasai, Y. The Diurnal Variation in Stratospheric Ozone from MACC Reanalysis , ERA-Interim , WACCM , and Earth Observation Data : Characteristics and Intercomparison **2021**.
83. North Atlantic Tracks - Flight Plan database. https://flightplandatabase.com/nav/NATS.
84. Kärcher, B.; Meilinger, S.K. Perturbation of the aerosol layer by aviation-produced aerosols: A parametrization of plume processes. *Geophysical Research Letters* **1998**, *25*, 4465–4468. doi:10.1029/1998GL900183.
85. Brunton, J. North Atlantic Skies – The gateway to Europe. https://nats.aero/blog/2014/06/north-atlantic-skies-gateway-europe/, 2014.
86. Air transport, passengers carried. https://data.worldbank.org/indicator/IS.AIR.PSGR.
87. Schumann, U.; Schlager, H.; Arnold, F.; Ovarlez, J.; Kelder, H.; Hov.; Hayman, G.; Isaksen, I.S.; Staehelin, J.; Whitefield, P.D. Pollution from aircraft emissions in the North Atlantic flight corridor: Overview on the POLINAT projects. *Journal of Geophysical Research Atmospheres* **2000**, *105*, 3605–3631. doi:10.1029/1999JD900941.
88. Thompson, A.M.; Singh, H.B.; Schlager, H. Introduction to special section: Subsonic assessment ozone and nitrogen oxide experiment (SONEX) and Pollution from aircraft emissions in the north atlantic flight corridor (POLINAT 2). *Journal of Geophysical Research: Atmospheres* **2000**, *105*, 3595–3603. doi:10.1029/2000JD900012.
89. on Climate Change, I.P., Anthropogenic and Natural Radiative Forcing. In *Climate Change 2013 – The Physical Science Basis: Working Group I Contribution to the Fifth Assessment Report of the Intergovernmental Panel on Climate Change*; Cambridge University Press, 2014; p. 659–740. doi:10.1017/CBO9781107415324.018.
90. Gettelman, A.; Pan, L.L.; Randel, W.J.; Hoor, P.; Birner, T.; Hegglin, M.I. the Extratropical Upper Troposphere and Lower Stratosphere. *Reviews of Geophysics* **2011**, *49*, 1–31. doi:10.1029/2011RG000355.1.INTRODUCTION.
91. Hoinka, K.P.; Reinhardt, M.E. North Atlantic Air Traffic Within the Lower Stratosphere: Cruising Times and Corresponding Emissions **1993**. *98*, 23,113–23,131.
92. Schumann, U. The impact of nitrogen oxides emissions from aircraft upon the atmosphere at flight altitudes - Results from the aeronox project. *Atmospheric Environment* **1997**, *31*, 1723–1733. doi:10.1016/S1352-2310(96)00326-3.
93. Johnson, C.; Henshaw, J.; Mclnnest, G. Impact of aircraft and surface emissions of nitrogen oxides on tropospheric ozone and global warming **1992**. *355*, 69–71.

94. Lee, D.; Pitari, G.; Grewe, V.; Gierens, K.; Penner, J.; Petzold, A.; Prather, M.; Schumann, U.; Bais, A.; Berntsen, T. Transport impacts on atmosphere and climate: Aviation. *Atmospheric Environment* **2010**, *44*, 4678–4734. doi:10.1016/j.atmosenv.2009.06.005.
95. Grewe, V.; Dameris, M.; Fichter, C.; Sausen, R. Impact of aircraft NOx emissions. Part 1: Interactively coupled climate-chemistry simulations and sensitivities to climate-chemistry feedback, lightning and model resolution. *Meteorologische Zeitschrift* **2002**, *11*, 177–186. doi:10.1127/0941-2948/2002/0011-0177.
96. Forster, C. The residence times of aircraft emissions in the stratosphere using a mean emission inventory and emissions along actual flight tracks. *Journal of Geophysical Research* **2003**, *108*, 8524. doi:10.1029/2002JD002515.
97. Fuglestvedt, J.S.; Berntsen, T.K.; Godal, O.; Sausen, R.; Shine, K.P.; Skodvin, T. Metrics of climate change: Assessing radiative forcing and emission indices. *Climatic Change* **2003**, *58*, 267–331. doi:10.1023/A:1023905326842.
98. Schneider, S.H. The Greenhouse Effect: Science and Policy. *Science* **1989**, *243*, 771–781. doi:10.1126/science.243.4892.771.
99. Archer, D.; Brovkin, V. The millennial atmospheric lifetime of anthropogenic CO2 **2008**. *90*, 283–297. doi:10.1007/s10584-008-9413-1.
100. Burkhardt, U.; Kärcher, B. Global radiative forcing from contrail cirrus. *Nature Climate Change* **2011**, *1*, 54–58. doi:10.1038/nclimate1068.
101. Schumann, U. Formation, properties and climatic effects of contrails. *Comptes Rendus Physique* **2005**, *6*, 549–565. doi:10.1016/j.crhy.2005.05.002.
102. Kärcher, B. Formation and radiative forcing of contrail cirrus. *Nature Communications* **2018**, *9*, 1824. doi:10.1038/s41467-018-04068-0.
103. Schmidt, E. Die Entstehung von Eisnebel aus den Auspuffgasen von Flugmotoren. *Schriften der Deutschen Akademie der Luftfahrtforschung* **1941**, *5*, 1–15.
104. Appleman, H. The Formation of Exhaust Condensation Trails by Jet Aircraft. *Bulletin of the American Meteorological Society* **1953**, *34*, 14–20. doi:10.1175/1520-0477-34.1.14.
105. Schumann, U. Contrails - a prototype of cirrus cloud studies since 80 years. *Meteorol. Zeitschrift* **1997**, *6*, 304–305.
106. Schumann, U. On conditions for contrail formation from aircraft exhausts. *Meteorologische Zeitschrift* **1996**, *5*, 4–23. doi:10.1127/metz/5/1996/4.
107. Tait, K. Assessing the effectiveness of contrail diversion schemes in mitigating aviation-induced climate change. Master's thesis, 2020.
108. Minnis, P.; Young, D.F.; Garber, D.P.; Nguyen, L.; Smith, W.L.; Palikonda, R. Transformation of contrails into cirrus during SUCCESS. *Geophysical Research Letters* **1998**, *25*, 1157–1160. doi:10.1029/97GL03314.
109. Spichtinger, P.; Leschner, M. Tellus B : Chemical and Physical Meteorology Horizontal scales of ice-supersaturated regions **2016**. *0889*.
110. Vertical spatial scales of ice supersaturation and probability of ice supersaturated layers in low resolution profiles of relative humidity. *DLR Deutsches Zentrum fur Luft- und Raumfahrt e.V. - Forschungsberichte* **2010**, pp. 239–243.
111. Schumann, U.; Graf, K.; Mannstein, H. Potential to reduce the climate impact of aviation by flight level changes. 3rd AIAA Atmospheric Space Environments Conference. American Institute of Aeronautics and Astronautics, 2011. doi:10.2514/6.2011-3376.
112. Schumann, U.; Heymsfield, A.J. On the Life Cycle of Individual Contrails and Contrail Cirrus. *Meteorological Monographs* **2017**, *58*, 3.1–3.24. doi:10.1175/AMSMONOGRAPHS-D-16-0005.1.
113. Newinger, C.; Burkhardt, U. Sensitivity of contrail cirrus radiative forcing to air traffic scheduling. *Journal of Geophysical Research Atmospheres* **2012**, *117*, 1–12. doi:10.1029/2011JD016736.
114. Kärcher, B.; Burkhardt, U.; Bier, A.; Bock, L.; Ford, I.J. The microphysical pathway to contrail formation. *Journal of Geophysical Research: Atmospheres* **2015**, *120*, 7893–7927. doi:10.1002/2015JD023491.
115. Kraabøl, A.G.; Stordal, F. Modelling chemistry in aircraft plumes 2: The chemical conversion of NO(x) to reservoir species under different conditions. *Atmospheric Environment* **2000**, *34*, 3951–3962. doi:10.1016/S1352-2310(00)00155-2.
116. Stevenson, D.S.; Doherty, R.M.; Sanderson, M.G.; Collins, W.J.; Johnson, C.E.; Derwent, R.G. Radiative forcing from aircraft NOx emissions: Mechanisms and seasonal dependence. *Journal of Geophysical Research D: Atmospheres* **2004**, *109*. doi:10.1029/2004JD004759.

117. Wild, O.; Prather, M.J.; Akimoto, H. Indirect from long-term global radiative emissions cooling. *October* **2001**, *28*, 1719–1722.
118. Myhre, G.; Shine, K.; Rädel, G.; Gauss, M.; Isaksen, I.; Tang, Q.; Prather, M.; Williams, J.; van Velthoven, P.; Dessens, O.; Koffi, B.; Szopa, S.; Hoor, P.; Grewe, V.; Borken-Kleefeld, J.; Berntsen, T.; Fuglestvedt, J. Radiative forcing due to changes in ozone and methane caused by the transport sector. *Atmospheric Environment* **2011**, *45*, 387–394. doi: 10.1016/j.atmosenv.2010.10.001.
119. Holmes, C.D.; Tang, Q.; Prather, M.J. Uncertainties in climate assessment for the case of aviation NO. *Proceedings of the National Academy of Sciences* **2011**, *108*, 10997–11002. doi: 10.1073/pnas.1101458108.
120. Myhre, G.; Nilsen, J.S.; Gulstad, L.; Shine, K.P.; Rognerud, B.; Isaksen, I.S. Radiative forcing due to stratospheric water vapour from CH4 oxidation. *Geophysical Research Letters* **2007**, *34*, 1–5. doi:10.1029/2006GL027472.
121. Jensen, E.J.; Toon, O.B.; Pfister, L.; Selkirk, H.B. Dehydration of the upper troposphere and lower stratosphere by subvisible cirrus clouds near the tropical tropopause. *Geophysical Research Letters* **1996**, *23*, 825–828. doi:10.1029/96GL00722.
122. Stenke, A.; Grewe, V. Simulation of stratospheric water vapor trends: Impact on stratospheric ozone chemistry. *Atmospheric Chemistry and Physics* **2005**, *5*, 1257–1272. doi: 10.5194/acp-5-1257-2005.
123. Miake-Lye, R.C.; Martinez-Sanchez, M.; Brown, R.C.; Kolb, C.E. Plume and wake dynamics, mixing, and chemistry behind a high speed civil transport aircraft. *Journal of Aircraft* **1993**, *30*, 467–479. doi:10.2514/3.46368.
124. Grooß, J.u.; Brühl, C.; Peter, T. Impact of aircraft emissions on tropospheric and stratospheric ozone. Part I. *Atmospheric Environment* **1998**, *32*, 3173–3184. doi: 10.1016/S1352-2310(98)00016-8.
125. Kawa, S.R.; Anderson, J.G.; Baughcum, S.L.; Brock, C.A.; Brune, W.H.; Cohen, R.C.; Kinnison, D.E.; Newman, P.A.; Rodriguez, J.M.; Stolarski, R.S.; others. Assessment of the effects of high-speed aircraft in the stratosphere: 1998. Technical report, National Aeronautics and Space Administration, 1999.
126. Gauss, M.; Isaken, I.S.; Wong, S.; Wang, W.C. Impact of H2O emissions from cryoplanes and kerosene aircraft on the atmosphere. *Journal of Geophysical Research: Atmospheres* **2003**, *108*, 1–11. doi:10.1029/2002jd002623.
127. Bond, T.C.; Doherty, S.J.; Fahey, D.W.; Forster, P.M.; Berntsen, T.; DeAngelo, B.J.; Flanner, M.G.; Ghan, S.; Kärcher, B.; Koch, D.; Kinne, S.; Kondo, Y.; Quinn, P.K.; Sarofim, M.C.; Schultz, M.G.; Schulz, M.; Venkataraman, C.; Zhang, H.; Zhang, S.; Bellouin, N.; Guttikunda, S.K.; Hopke, P.K.; Jacobson, M.Z.; Kaiser, J.W.; Klimont, Z.; Lohmann, U.; Schwarz, J.P.; Shindell, D.; Storelvmo, T.; Warren, S.G.; Zender, C.S. Bounding the role of black carbon in the climate system: A scientific assessment. *Journal of Geophysical Research: Atmospheres* **2013**, *118*, 5380–5552. doi:10.1002/jgrd.50171.
128. Brown, R.C.; Anderson, M.R.; Miake-Lye, R.C.; Kolb, C.E.; Sorokin, A.A.; Buriko, Y.Y. Aircraft exhaust sulfur emissions. *Geophysical Research Letters* **1996**, *23*, 3603–3606. doi: https://doi.org/10.1029/96GL03339.
129. Penner, J.E.; Zhou, C.; Garnier, A.; Mitchell, D.L. Anthropogenic Aerosol Indirect Effects in Cirrus Clouds. *Journal of Geophysical Research: Atmospheres* **2018**, *123*, 11,652–11,677. doi: 10.1029/2018JD029204.
130. Randall, D.; Wood, R.; Bony, S.; Colman, R.; Fichefet, T.; Fyfe, J.; Kattsov, V.; Pitman, A.; Srinivasan, J.; Ronald, S.; Sumi, A.; Taylor, K., Climate Models and Their Evaluation; 2007; pp. 590–662.
131. Wilkerson, J.T.; Jacobson, M.Z.; Malwitz, A.; Balasubramanian, S.; Wayson, R.; Fleming, G.; Naiman, A.D.; Lele, S.K. Analysis of emission data from global commercial aviation: 2004 and 2006. *Atmospheric Chemistry and Physics* **2010**, *10*, 6391–6408. doi: 10.5194/acp-10-6391-2010.
132. Fuglestvedt, J.; Shine, K.; Berntsen, T.; Cook, J.; Lee, D.; Stenke, A.; Skeie, R.; Velders, G.; Waitz, I. Transport impacts on atmosphere and climate: Metrics. *Atmospheric Environment* **2010**, *44*, 4648–4677. doi:10.1016/j.atmosenv.2009.04.044.
133. Cain, M.; Lynch, J.; Allen, M.R.; Fuglestvedt, J.S.; Frame, D.J.; Macey, A.H. Improved calculation of warming-equivalent emissions for short-lived climate pollutants. *npj Climate and Atmospheric Science* **2019**, *2*, 29. doi:10.1038/s41612-019-0086-4.

134. Stevens, B.; Giorgetta, M.; Esch, M.; Mauritsen, T.; Crueger, T.; Rast, S.; Salzmann, M.; Schmidt, H.; Bader, J.; Block, K.; Brokopf, R.; Fast, I.; Kinne, S.; Kornblueh, L.; Lohmann, U.; Pincus, R.; Reichler, T.; Roeckner, E. Atmospheric component of the MPI-M earth system model: ECHAM6. *Journal of Advances in Modeling Earth Systems* **2013**, *5*, 146–172. doi: 10.1002/jame.20015.
135. Bock, L.; Burkhardt, U. Contrail cirrus radiative forcing for future air traffic. *Atmospheric Chemistry and Physics Discussions* **2019**, pp. 1–22. doi:10.5194/acp-2018-1294.
136. Neale, R.B.; Chen, C.c.; Lauritzen, P.H.; Williamson, D.L.; Conley, A.J.; Smith, A.K.; Mills, M.; Morrison, H. Description of the NCAR Community Atmosphere Model (CAM 5.0). Technical report, National Center for Atmospheric Research (NCAR), 2004.
137. Cooke, M. Global Modelling of Atmospheric Trace Gases using the CRI Mechanism. PhD thesis, University of Bristol, 2010.
138. Jenkin, M.; Watson, L.; Utembe, S.; Shallcross, D. A Common Representative Intermediates (CRI) mechanism for VOC degradation. Part 1: Gas phase mechanism development. *Atmospheric Environment* **2008**, *42*, 7185–7195. doi:10.1016/j.atmosenv.2008.07.028.
139. Emmons, L.K.; Walters, S.; Hess, P.G.; Lamarque, J.F.; Pfister, G.G.; Fillmore, D.; Granier, C.; Guenther, A.; Kinnison, D.; Laepple, T.; Orlando, J.; Tie, X.; Tyndall, G.; Wiedinmyer, C.; Baughcum, S.L.; Kloster, S. Description and evaluation of the Model for Ozone and Related chemical Tracers, version 4 (MOZART-4). *Geoscientific Model Development* **2010**, *3*, 43–67. doi: 10.5194/gmd-3-43-2010.
140. Freeman, S.J.; Lim, L.L.; Lee, D.S. Examining the effect of aviation NOx emissions as a short-lived climate-forcer: Assessing the linearity of the NOx -O3 chemical system. PhD thesis, Manchester Metropolitan University, 2017.
141. Roelofs, G.J. Intercomparison of tropospheric ozone models: Ozone transport in a complex tropopause folding event. *Journal of Geophysical Research* **2003**, *108*, 8529. doi: 10.1029/2003JD003462.
142. Stone, D.; Whalley, L.K.; Heard, D.E.; Stone, D. Tropospheric OH and HO 2 radicals: field measurements and model comparisons. *Chemical Society Reviews* **2012**, *41*, 6348–6404. doi: 10.1039/c2cs35140d.
143. Monks, P.S. Gas-phase radical chemistry in the troposphere. *Chemical Society Reviews* **2005**, *34*, 376. doi:10.1039/b307982c.
144. Prinn, R.G. The Cleansing Capacity of the Atmosphere. *Annual Review of Environment and Resources* **2003**, *28*, 29–57. doi:10.1146/annurev.energy.28.011503.163425.
145. Jenkin, M.E.; Clemitshaw, K.C. Ozone and other secondary photochemical pollutants: chemical processes governing their formation in the planetary boundary layer. *Atmospheric Environment* **2000**, *34*, 2499–2527. doi:https://doi.org/10.1016/S1352-2310(99)00478-1.
146. Dodge, M. Combined use of modeling techniques and smog chamber data to derive ozone-precursor relationship. Proceedings of the international conference on photochemical oxidant pollution and its control. U.S. Environmental Protection Agency, 1977, Vol. 2, pp. 881–889.
147. Thompson, A.M. The oxidizing capacity of the Earth's atmosphere: Probable past and future changes. *Science* **1992**, *256*, 1157–1165. doi:10.1126/science.256.5060.1157.
148. Jacob, D.J., Introduction to Atmospheric Chemistry; Princeton University Press, 1999; chapter 11 Oxidising Power of the Troposphere.
149. Gunz, D.W.; Hoffmann, M.R. Atmospheric chemistry of peroxides: a review. *Atmospheric Environment. Part A. General Topics* **1990**, *24*, 1601–1633. doi:10.1016/0960-1686(90)90496-A.
150. Khan, M.A.H.; Miles, B.; Jenkin, M.E.; Derwent, R.G.; Percival, C.J.; Shallcross, D.E. Investigating the Impacts of Nonacyl Peroxy Nitrates on the Global Composition of the Troposphere Using a 3-D Chemical Transport Model, STOCHEM-CRI. *ACS Earth and Space Chemistry* **2020**, *4*, 1201–1212. doi:10.1021/acsearthspacechem.0c00133.
151. Song, C.H. Dispersion and chemical evolution of ship plumes in the marine boundary layer: Investigation of O 3 /NO y /HO x chemistry. *Journal of Geophysical Research* **2003**, *108*, 4143. doi:10.1029/2002JD002216.
152. Kraabøl, A.G.; Berntsen, T.K.; Sundet, J.K.; Stordal, F. Impacts of NOx emissions from subsonic aircraft in a global three-dimensional chemistry transport model including plume processes. *Journal of Geophysical Research Atmospheres* **2002**, *107*. doi:10.1029/2001JD001019.
153. Meijer, E.W.; Van Velthoven, P.F.; Wauben, W.M.; Beck, J.P.; Velders, G.J. The effects of the conversion of nitrogen oxides in aircraft exhaust plumes in global models. *Geophysical Research Letters* **1997**, *24*, 3013–3016. doi:10.1029/97GL53156.

154. Jacob, D.J. Heterogeneous chemistry and tropospheric ozone. *Atmospheric Environment* **2000**, *34*, 2131–2159. doi:10.1016/S1352-2310(99)00462-8.
155. Meilinger, S.K.; Kärcher, B.; Peter, T. Microphysics and heterogeneous chemistry in aircraft plumes - high sensitivity on local meteorology and atmospheric composition. *Atmospheric Chemistry and Physics* **2005**, *5*, 533–545. doi:10.5194/acp-5-533-2005.
156. Perry, K.D.; Hobbs, P.V. Further evidence for particle nucleation in clear air adjacent to marine cumulus clouds. *Journal of Geophysical Research* **1994**, *99*. doi:10.1029/94jd01926.
157. Kärcher, B.; Hirschberg, M.M.; Fabian, P. Small-scale chemical evolution of aircraft exhaust species at cruising altitudes. *Journal of Geophysical Research: Atmospheres* **1996**, *101*, 15169–15190. doi:10.1029/96JD01059.
158. Kärcher, B.; Peter, T.; Biermann, U.M.; Schumann, U. The initial composition of jet condensation trails. *Journal of the Atmospheric Sciences* **1996**, *53*, 3066–3083. doi: 10.1175/1520-0469(1996)053<3066:TICOJC>2.0.CO;2.
159. Heymsfield, A.; Baumgardner, D.; DeMott, P.; Forster, P.; Gierens, K.; Kärcher, B. Contrail Microphysics. *Bulletin of the American Meteorological Society* **2010**, *91*, 465–472. doi: 10.1175/2009BAMS2839.1.
160. Meerkötter, R.; Schumann, U.; Doelling, D.R.; Minnis, P.; Nakajima, T.; Tsushima, Y. Radiative forcing by contrails. *Annales Geophysicae* **1999**, *17*, 1080–1094. doi: 10.1007/s00585-999-1080-7.
161. Schumann, U. A contrail cirrus prediction model. *Geoscientific Model Development* **2012**, *5*, 543–580. doi:10.5194/gmd-5-543-2012.
162. Bickel, M.; Ponater, M.; Bock, L.; Burkhardt, U.; Reineke, S. Estimating the Effective Radiative Forcing of Contrail Cirrus. *Journal of Climate* **2020**, *33*, 1991–2005. doi: 10.1175/JCLI-D-19-0467.1.
163. Kärcher, B. Aviation-produced aerosols and contrails. *Surveys in Geophysics* **1999**, *20*, 113–167. doi:10.1023/A:1006600107117.
164. Schumann, U.; Mayer, B.; Graf, K.; Mannstein, H. A parametric radiative forcing model for contrail cirrus. *Journal of Applied Meteorology and Climatology* **2012**, *51*, 1391–1406. doi: 10.1175/JAMC-D-11-0242.1.
165. Wennberg, P.O.; Hanisco, T.F.; Jaeglé, L.; Jacob, D.J.; Hintsa, E.J.; Lanzendorf, E.J.; Anderson, J.G.; Gao, R.S.; Keim, E.R.; Donnelly, S.G.; Negro, L.A.D.; Fahey, D.W.; McKeen, S.A.; Salawitch, R.J.; Webster, C.R.; May, R.D.; Herman, R.L.; Proffitt, M.H.; Margitan, J.J.; Atlas, E.L.; Schauffler, S.M.; Flocke, F.; McElroy, C.T.; Bui, T.P. Hydrogen Radicals, Nitrogen Radicals, and the Production of O 3 in the Upper Troposphere. *Science* **1998**, *279*, 49–53. doi: 10.1126/science.279.5347.49.
166. Jaeglé, L. Chemistry of HOx radicals in the upper troposphere. *Atmospheric Environment* **2001**, *35*, 469–489. doi:10.1016/S1352-2310(00)00376-9.
167. Unterstrasser, S.; Gierens, K. Numerical simulations of contrail-to-cirrus transition – Part 1: An extensive parametric study. *Atmospheric Chemistry and Physics* **2010**, *10*, 2017–2036. doi: 10.5194/acp-10-2017-2010.
168. Unterstrasser, S. The contrail mitigation potential of aircraft formation flight derived from high-resolution simulations. *Aerospace* **2020**, *7*, 1–22. doi:10.3390/aerospace7120170.
169. Flightradar24 AB. Live flight tracker - real-time flight tracker map.
170. Paoli, R. Modeling Emissions from Concentrated Sources into Large-Scale Models: Theory and apriori Testing. *Atmosphere* **2020**, *11*, 863. doi:10.3390/atmos11080863.
171. Burkhardt, U.; Karcher, B. Process-based simulation of contrail cirrus in a global climate model. *Journal of Geophysical Research Atmospheres* **2009**, *114*, 1–13. doi: 10.1029/2008JD011491.
172. Meilinger, S.K.; Kärcher, B.; Peter, T. Suppression of chlorine activation on aviation-produced volatile particles. *Atmospheric Chemistry and Physics* **2002**, *2*, 307–312. doi: 10.5194/acp-2-307-2002.
173. Burkhardt, U.; Kärcher, B.; Schumann, U. Global Modeling of the Contrail and Contrail Cirrus Climate Impact. *Bulletin of the American Meteorological Society* **2010**, *91*, 479–484. doi: 10.1175/2009BAMS2656.1.
174. Lee, D.S.; Fahey, D.W.; Forster, P.M.; Newton, P.J.; Wit, R.C.; Lim, L.L.; Owen, B.; Sausen, R. Aviation and global climate change in the 21st century. *Atmospheric Environment* **2009**, *43*, 3520–3537. doi:10.1016/j.atmosenv.2009.04.024.

175. Bock, L.; Burkhardt, U. The temporal evolution of a long-lived contrail cirrus cluster: Simulations with a global climate model. *Journal of Geophysical Research: Atmospheres* **2016**, *121*, 3548–3565. doi:10.1002/2015JD024475.

Author Contributions: For research articles with several authors, a short paragraph specifying their individual contributions must be provided. The following statements should be used "Conceptualization, X.X. and Y.Y.; methodology, X.X.; software, X.X.; validation, X.X., Y.Y. and Z.Z.; formal analysis, X.X.; investigation, X.X.; resources, X.X.; data curation, X.X.; writing—original draft preparation, X.X.; writing—review and editing, X.X.; visualization, X.X.; supervision, X.X.; project administration, X.X.; funding acquisition, Y.Y. All authors have read and agreed to the published version of the manuscript.", please turn to the CRediT taxonomy for the term explanation. Authorship must be limited to those who have contributed substantially to the work reported.

Funding: Please add: "This research received no external funding" or "This research was funded by NAME OF FUNDER grant number XXX." and and "The APC was funded by XXX". Check carefully that the details given are accurate and use the standard spelling of funding agency names at https://search.crossref.org/funding, any errors may affect your future funding.

Institutional Review Board Statement: In this section, please add the Institutional Review Board Statement and approval number for studies involving humans or animals. Please note that the Editorial Office might ask you for further information. Please add "The study was conducted according to the guidelines of the Declaration of Helsinki, and approved by the Institutional Review Board (or Ethics Committee) of NAME OF INSTITUTE (protocol code XXX and date of approval)." OR "Ethical review and approval were waived for this study, due to REASON (please provide a detailed justification)." OR "Not applicable" for studies not involving humans or animals. You might also choose to exclude this statement if the study did not involve humans or animals.

Informed Consent Statement: Any research article describing a study involving humans should contain this statement. Please add "Informed consent was obtained from all subjects involved in the study." OR "Patient consent was waived due to REASON (please provide a detailed justification)." OR "Not applicable" for studies not involving humans. You might also choose to exclude this statement if the study did not involve humans.
Written informed consent for publication must be obtained from participating patients who can be identified (including by the patients themselves). Please state "Written informed consent has been obtained from the patient(s) to publish this paper" if applicable.

Data Availability Statement: In this section, please provide details regarding where data supporting reported results can be found, including links to publicly archived datasets analyzed or generated during the study. Please refer to suggested Data Availability Statements in section "MDPI Research Data Policies" at https://www.mdpi.com/ethics. You might choose to exclude this statement if the study did not report any data.

Acknowledgments: Thibaud M. Fritz (MIT), Stephen Roome,

Conflicts of Interest: Declare conflicts of interest or state "The authors declare no conflict of interest." Authors must identify and declare any personal circumstances or interest that may be perceived as inappropriately influencing the representation or interpretation of reported research results. Any role of the funders in the design of the study; in the collection, analyses or interpretation of data; in the writing of the manuscript, or in the decision to publish the results must be declared in this section. If there is no role, please state "The funders had no role in the design of the study; in the collection, analyses, or interpretation of data; in the writing of the manuscript, or in the decision to publish the results".

Sample Availability: Samples of the compounds ... are available from the authors.

Abbreviations

The following abbreviations are used in this manuscript:

MDPI	Multidisciplinary Digital Publishing Institute
DOAJ	Directory of open access journals
TLA	Three letter acronym
LD	Linear dichroism

Appendix A

Appendix A.1

The appendix is an optional section that can contain details and data supplemental to the main text—for example, explanations of experimental details that would disrupt the flow of the main text but nonetheless remain crucial to understanding and reproducing the research shown; figures of replicates for experiments of which representative data are shown in the main text can be added here if brief, or as Supplementary Data. Mathematical proofs of results not central to the paper can be added as an appendix.

Table A1. This is a table caption. Tables should be placed in the main text near to the first time they are cited.

Title 1	Title 2	Title 3
Entry 1	Data	Data
Entry 2	Data	Data

All appendix sections must be cited in the main text. In the appendices, Figures, Tables, etc. should be labeled, starting with "A"—e.g., Figure A1, Figure A2, etc.